Water Resources and Industry 29 (2023) 100211

Contents lists available at ScienceDirect

Water Resources and Industry

journal homepage: www.elsevier.com/locate/wri

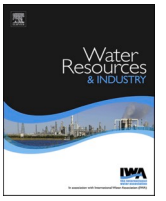

Band engineering of BiOBr based materials for photocatalytic wastewater treatment via advanced oxidation processes (AOPs) – A review

Zohaib Saddique [a], Muhammad Imran [a,**], Ayesha Javaid [a], Shoomaila Latif [b], Nazim Hussain [c], Przemysław Kowal [d], Grzegorz Boczkaj [d,e,*]

[a] Centre for Inorganic Chemistry, School of Chemistry, University of the Punjab Lahore, 54000, Pakistan
[b] School of Physical Sciences, University of the Punjab, Lahore, 54000, Pakistan
[c] Centre of Excellence in Applied Molecular Biology, University of the Punjab Lahore, 54000, Pakistan
[d] Department of Sanitary Engineering, Faculty of Civil and Environmental Engineering, Gdańsk University of Technology, 11/12 Narutowicza Str., Gdańsk, 80-233, Poland
[e] EkoTech Center, Gdańsk University of Technology, G. Narutowicza St. 11/12, Gdansk, 80-233, Poland

ARTICLE INFO

Keywords:
Bismuth oxybromide
BiOBr composites
Nanomaterials
Heterojunction
Heterogeneous catalysis
Radicals

ABSTRACT

Semiconductor based photocatalysts have been an efficient technology for water and wastewater remediation, addressing the concepts of green chemistry and sustainable development. Owing to narrow and suitable band structure, BiOBr is a promising candidate for efficient wastewater treatment via photocatalysis. Enhancement of photocatalytic properties can be obtained by various techniques like doping, element rich strategy, facet engineering, and defect control. This review primarily focuses on the band engineering of single BiOBr, its binary, ternary composites and their applications in degradation of hazardous pollutants in wastewater. Moreover, current challenges and future perspectives were discussed along with concluding comments.

1. Introduction

Industrialization has been a beneficial factor in our lives but, it is also caused of environmental pollution including air, water and soil pollution. The rapid increase in the population has increased this pollution particularly, water pollution, which is a major challenge that is threatening the existence of the human world [1,2]. Reports suggest the presence of a variety of pollutants in wastewater including pharmaceuticals, heavy metals, dyes and other organic pollutants [3–6]. These contaminants create huge problems for the environment in general and the human population in particular. Reportedly, there is an abundance of pharmaceutical products, such as antibiotics and other drugs, in water bodies, and it results in the generation of antibiotics resistance among bacteria, rendering them ineffective and also cause major health risks to humankind [7,8]. Limited exposure to heavy metals has minimal effect on environment, but long term exposure is hazardous for humans leading to the failure of human body systems. Most of the heavy metals are carcinogenic and they cause skin diseases, kidney failure, lung damage and fragility of bones [4,9]. Dyes present in the wastewater are toxic

* Corresponding author. Department of Sanitary Engineering, Faculty of Civil and Environmental Engineering, Gdańsk University of Technology, 11/12 Narutowicza Str., Gdańsk, 80-233, Poland.
** Corresponding author.
E-mail addresses: imran.hons@pu.edu.pk (M. Imran), grzegorz.boczkaj@pg.edu.pl (G. Boczkaj).

https://doi.org/10.1016/j.wri.2023.100211
Received 8 March 2023; Received in revised form 13 April 2023; Accepted 24 April 2023
Available online 25 April 2023

to aquatic life and cause cancers in human beings [10–12]. Summarily, dyes containing wastewater is highly hazardous for ecosystem and the health of living beings, it should be treated before entering into water bodies. It is a prerequisite for good human health to drink clean water free from toxic materials such as pharmaceuticals, dyes, heavy metals, organic waste and harmful microorganisms. A report published by the United Nations on world water development suggests an increase in the demand for clean water by nearly one-third in next 30 years [13]. Other than primary requirement of clean water for human health, various industries such as food, electronics and pharmaceuticals also need clean and potable water for their proper functioning [8,14]. To reduce the health risks, environmental hazards and to meet world water demands, it is needed to effectively treat the wastewater. However, conventional techniques for wastewater remediation process are not efficient enough to remove emerging pollutants such as pharmaceuticals, dyes, and organic pollutants [15,16]. Owing to the failure of conventional wastewater treatment plants in handling of aforementioned contaminants it is essentially needed to develop new technologies for proper removal of these hazardous materials [17]. For wastewater treatment aimed at removal of these chemically stable, highly persistent and non-biodegradable contaminants, various advanced technologies have been employed. These advanced wastewater treatment technologies include electrochemical reduction [18], membrane filtration [12,19], precipitation [20], electrodialysis [21], photocatalysis [22,23] and electrodeionization [24]. These technologies except photocatalysis are not suitable for wastewater treatment in terms of efficiency and economy. Large intake of energy, complicated process, wastes and by-products formation are the major disadvantages of these techniques. Among all of these, photocatalysis is the best technique owing to its efficiency and cost-effectiveness. Photocatalysis is the process in which of sunlight energy is converted into chemical energy, through a series of reaction steps, that is further used to degrade the pollutants in wastewater. It converts complex pollutants into simple and harmless molecules using mild conditions and consuming abundantly available sunlight. These features make this technique very economical and environment friendly [22,25]. Photocatalysis is a state of the art oxidation process and it mechanism involves generation of electrons and holes after striking of sunlight photon on the surface of photocatalyst. Degradation reaction of wastewater contaminant is initiated by electrons and holes that are photogenerated in valence and conduction band, respectively [23,26]. Suitable properties of semiconductor photocatalyst determine rate and efficiency of photocatalysis. Therefore, an ideal catalyst must be chemically/biologically stable, photo-active, cost-effective, photo-stable, and reusable and must have a narrowband gap so that it can harvest the maximum portion of sunlight energy in broad spectrum.

Owing to the importance of photocatalysis, the developments and improvements in the properties of photocatalyst are widely researched areas in this field, as exhibited by excellent reviews referenced here [27–29]. Owing to the beneficial presence of oxygen in photocatalyst, various metal oxide semiconductors including Fe_2O_3 [30], TiO_2 [3,31,32], ZnO [33], Bi_2O_3–ZnO heterojunction [34], Bi^{3+}/ZnO [35], Ce_2O_3 [36], BiFeO3 [37] and bismuth oxyhalides BiOX (X = Cl, Br, I) based photocatalysts have been synthesized aimed at photocatalytic wastewater treatment [28,38,39]. As compared to the conventional metal oxides, BiOX offers more suitable properties for efficient photocatalytic process such as better chemical stability, biological inertness, better positioned band structure, narrowband gap for maximum sunlight energy harvesting and unique layered structure that enhances rate of photocatalysis [40]. BiOX has unique lamellar structure in which X_2^{2-} slabs are interleaving Bi_2O_2 layers and Bi-X show weak van der Waals interaction and Bi–O strongly bonded through covalent bond as shown in Fig. 1. This novel structure supports the production of electric field internally that acts as facilitator for more charge separation and enhancing overall photocatalytic process [41,42].

Among BiOX, BiOBr is an ideal photocatalyst owing to its small band gap (2.75 eV) [43], making it capable of maximum visible sunlight energy harvesting photocatalyst [44]. BiOCl has a broad band gap of 3.3 eV with strong absorption in UV region light while bismuth oxyiodide (BiOI) has a small band gap of 1.77 eV and it is a visible light active photocatalyst. Although, BiOBr and BiOI both have narrowband gap, but there is a high recombination frequency of charges in BiOI that results in decimation of energy without effective photocatalytic activity. The effectiveness of a photocatalyst is determined by its capability to absorb light and utilize that light energy to excite electrons from valence and these electrons jump to the conduction band followed by creation of holes in the former

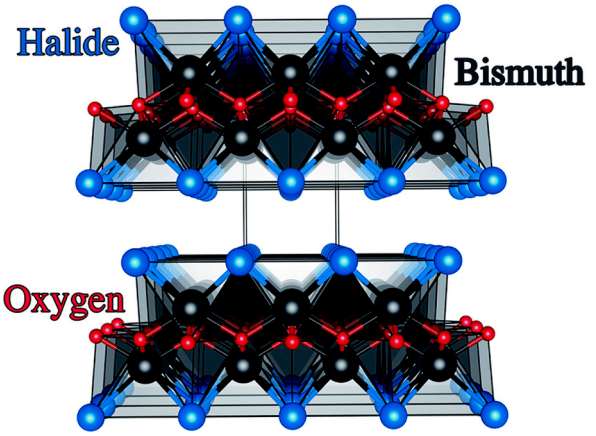

Fig. 1. Unique lamellar structure of BiOX illustrating the presence of X_2^{2-}slabs between Bi_2O_2 layers. Reproduced from Ref. [41] with permission from the Royal Society of Chemistry. This is an Open Access Article licensed under Creative Commons Attribution 3.0 Unported Licence. https://creativecommons.org/licenses/by/3.0/.

band, provided that band gap of semiconductors is equal to or less than absorbed light. These generated electron hole pairs initiate chemical reaction that degrade contaminants in the wastewater treatment process. Other than band gap, the efficiency of photocatalyst is also influenced by the speed with which electrons and holes pair recombine, the swift recombination of charges decreases the photocatalytic performance [45–49]. Conclusively, Bismuth oxybromide (BiOBr) is the most efficient photocatalyst as it has a suitably small band gap (2.75 eV) [43] and suitable band structure that minimize rapid recombination of electrons and holes; however this rate is not suitable for large scale applications. However, there are some shortcomings that restrict practical applications of single BiOBr at large scale wastewater treatment. These shortcomings include rapid recombination rate and less separation of photo-generated charge carriers, poor sunlight utilization, and difficult recovery of catalyst for reuse [50]. Various methods have been developed, to overcome these limitations, such as photosensitization, facet control, defect engineering, doping, bismuth rich strategy and heterojunction formation etc. In photosensitization, a photosensitizer such as metal porphyrin or phthalocyanine is introduced with BiOBr to generate a heterostructure photocatalyst with better charge separation and visible light absorption [51]. To maximize the reactive surface of photocatalyst, facet control strategy is used such as formation of nanosheets which enhance the exposed reactive sites and narrow the band gap of BiOBr photocatalyst [52]. In defect engineering, metal-oxygen vacancies are created to modulate absorption range, enhance charge separation and increase active site area, for example, introduction of bismuth vacancy in BiOBr nanosheets reduced the charge carrier recombination rate and enhanced the photocatalytic performance. To address the rapid recombination of electrons and holes, transition metals are introduced as dopants, yttrium doping on BiOBr can increase about 17% of photocatalytic performance in degradation of ciprofloxacin [53]. To increase the surface area and narrow down the band gap, a bismuth-rich strategy is commonly used [54]. The formation of heterojunctions of BiOBr with other materials such SnS_2 and Bi_2S_3 enhances the electron-hole separation and increases photocatalytic activity [48,55]. In the process of heterojunction formation, two or more semiconductors with compatible band structure and band gap are coupled to take photocatalytic process at higher level for wastewater treatment. Various studies on heterojunction formation portray this method as a most suitable solution to overcome the aforementioned shortcomings of semiconductor photocatalyst.

Recently, heaps of work has been reported on the binary and ternary composites aimed at improving photocatalytic efficiency of BiOBr photocatalyst [49,56–58]. There is limitation in binary composites that transfer of electron-hole pairs and its participation in redox reaction is quite a complicated process and causes lagging in overall degradation reaction. To overcome this limitation, researchers gave more focus to the design and development of ternary composites having improved efficiency intrinsically. Ternary composites are better than binary composites in terms of providing more active sites and suppressing the recombination of photo-induced charges [59–63]. The significance of BiOBr in photocatalytic wastewater treatment is increased by its maximum visible light harvesting capability coupled with more reactive sites and suppressed electron-hole pair recombination phenomenon.

To date, according to our knowledge, no review has been published focusing on binary and ternary composites of BiOBr as a photocatalyst for wastewater treatment. The purpose of this review is to elaborate recent research on binary and ternary composites of BiOBr with primary focus on band engineering for maximizing its photocatalytic efficiency. The hazardous effects of wastewater pollutants on the environment and human health are also critically analyzed while outlining synthesis approaches for binary and ternary BiOBr composites for addressing this environmental issue. This review provides elaborative information to the reader about band gap engineering techniques, particularly heterojunction formation and significance of this technique in the application of BiOBr binary and ternary composites for photocatalytic wastewater treatment.

2. Synthesis of BiOBr composites

The combination of two or three semiconductors has been successful in enhancing light harvesting capacity, increasing charge separation, providing more active sites and suppressing charge recombination. The coupling of semiconductors having compatible band structures results in the synergistic role of each semiconductor used and enhances the surface area, ultimately leading to improvement in photocatalytic efficiency of composites. BiOBr based binary and ternary composites have been prepared mainly by

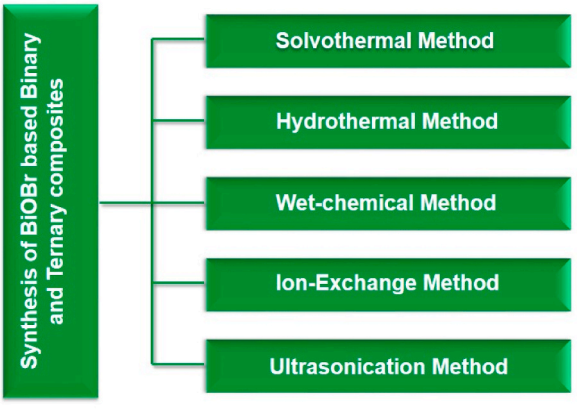

Fig. 2. Various synthesis methods of bismuth oxybromide based binary and ternary photocatalyst.

solvothermal [54], ultrasonication [64], ion exchange [65], wet chemical [66], co-precipitation [67] and hydrothermal methods [68], as exhibited in Fig. 2. The subsequent paragraphs give a brief outlook of these synthetic methods.

2.1. Solvothermal method

In solvothermal method, the precursors are treated with heat at high pressure generated in an autoclave. This autogenous pressure is the main reason for the initiation of a reaction that was not possible to achieve at normal pressure. A variety of the solvents are used to produce precursor solutions such as ethylene glycol [50], ethanol [69] and glycerol [70]. For instance, CdS/BiOBr binary composites have been synthesized using solvothermal route in which ethylene glycol is used as solvent and the product was employed for degradation of ciprofloxacin and norfloxacin antibiotics [71]. Li and coworker reported synthesis of Fe_3O_4/BiOBr/BiOI ternary composites through solvothermal method employing ethylene glycol as solvent and studies their photocatalytic activity by degrading chemical dye rhodamine B [50]. Solvothermal approach offers high crystal quality, uniform particle size and high yield. Other BiOBr based composites synthesized through solvothermal method include PANI/BiOBr/$ZnFe_2O_4$ [72], Fe_3O_4/mSiO_2/BiOBr [69] and BiOCl/BiOBr [73].

2.2. Ultrasonication method

In this method, reaction mixtures undergo ultrasonic processing for a suitable time. Qu et al. synthesized K/g-C_3N_4/BiOBr ternary system through ultrasonication of reaction mixture. K/g-C_3N_4 was ultrasonicated before addition of bismuth nitrate, as a precursor, and cetyl trimethyl ammonium bromide (CTAB), as a surfactant, in suspension. The reaction mixture was heated in a water bath for 2 h at 80 °C. Excessive CTAB and other impurities were removed by washing with ultrapure water and alcohol [64]. Cheng et al. synthesized BiOBr/$Bi_2O_2CO_3$ binary composite through same route in ultrasonication of only 40 min after mixing sodium bromide in deionized water and then dispersing $Bi_2O_2CO_3$. The pH of the solution determined the surface area of the product, pH = 2 was ideal for preparing photocatalyst with highest efficiency [74]. This method demands high edge technologies, resulting in the high cost of photocatalyst synthesis.

2.3. Ion exchange method

In this method, already present ionic species in the material template are replaced by desired chemical species leading to the formation of new product. Lyu et al. [65] synthesized Bi/BiOBr/AgBr by employing ion exchange method in which Br/BiOBr was added in ethylene glycol solution of $AgNO_3$ and stirred for 12 h. To collect the product, centrifugation was employed and it was dried for several hours at 80 °C before using it as a photocatalyst to degrade of rhodamine B. Similarly, AgBr/g-C_3N_4/BiOBr based ternary photocatalyst was also synthesized through ion exchange rout, which was employed for the photocatalytic degradation of industrial dyes and pharmaceutical products present in wastewater [75].

2.4. Wet-chemical method

This method is simple liquid phase synthesis of composites in deionized water or any other suitable liquid. Li et al. employed this method in the synthesis of Ag/BiOBr/GO in which separate solutions of BiOBr and $AgNO_3$ were blended together and stirred for 10–15 min. Graphene oxide and $NaBH_4$ were added to the reaction mixture and stirred for 1 h. To wash the product, ultrapure water was used and it was oven dried for 24–48 h at 60 °C [66]. Gao et al. reported the synthesis of $BiPO_4$/BiOBr binary composites by mixing BiOBr in ethanol and adding phosphoric acid (H_3PO_4) dropwise with continuous vigorous stirring for 20 min. The product was obtained in the form of precipitates that were washed several times and placed in an oven at 80 °C for 12 h [76]. It has been known that toxicity and by-product formation are major limitations of this method.

2.5. Co-precipitation method

In co-precipitation method, the components are precipitated simultaneously with the help of co-precipitating agent such as $NaBH_4$. This method is environment friendly in terms of its less time consumption and requirement of low temperature, as compared to other methods. Guo et al. synthesized Ag/CDots/BiOBr through this method. It involved the dispersion of CDots/BiOBr in deionized water with $AgNO_3$ and then the reaction mixture was vigorously stirred until a suspension was formed. The dropwise addition of $NaBH_4$ solution in the suspension resulted in the co-precipitation of product that was separated after centrifugation. The product was employed to degrade 4-chlorophenol, wastewater contaminant, through photocatalysis under sunlight [67]. In the co-precipitation method, nucleation and product growth kinetics can be controlled by manipulating release of component ions. Similarly, BiOBr/BiOCl/PANI was synthesized by the same method and the product was employed for degradation of wastewater abundant dye methyl orange [77]. Other composite synthesized through co-precipitation route is BiOBr/TiO_2 [78].

2.6. Hydrothermal method

There is a slight difference of employed solvent between solvothermal methods where various organic solvents are used, while in hydrothermal route water is employed as a solvent. Normally, precursors are dissolved in distilled water and transferred into an

autoclave followed by heating for a suitable time and temperature, autogenous pressure initiates the reaction and a variety of heterostructures are produced. Time and temperature of reaction, precursor and medium of solution are major determining factors for the quality of product. Jiang et al. synthesized BiOBr/BiOI binary composites through a hydrothermal method in which precursors were mixed in water/nitric acid and then heated for 12 h at temperature ranging from 110 to 260 °C. The product with varying ratios of oxygen and halides were employed for the photocatalytic degradation of wastewater contaminants such as phenols and crystal violet dyes [68]. Ternary composites of BiOBr/Fe_3O_4/rGO were also synthesized by the hydrothermal method, as shown in Fig. 3 [62]. Hydrothermal synthesis is cost effective, less toxic and controllable in terms of size and morphology. Other BiOBr composites synthesized by hydrothermal method include AgBr/g-C_3N_4/BiOBr [75], CQDs/BiOCl/BiOBr [79], BiOCl/BiOBr [80] and Bi_2S_3/BiOBr [81].

3. Photocatalysis

Photocatalysis is a phenomenon in which a semiconductor based photocatalyst is employed to absorb sunlight and initiates the degradation reaction. Sunlight energy is converted into chemical energy that is used to degrade a variety of pollutants including organic molecules, dyes, pharmaceuticals, pesticides, personal care products, oils and inorganic molecules [82–84]. Electrons, excited by sunlight energy, jump from the valence band, to the conduction band, followed by the creation of holes in the same band; this excitation requires striking of sunlight photons on the photocatalyst surface, provided that they have energy more than the band gap of the photocatalyst. The energy consumed by this process is provided by the sunlight photons. Semiconductor with narrowband gap such as BiOBr [85] is more suitable the photocatalyst because narrow band gap enables photocatalyst to harvest the maximum visible sunlight portion. Photo excited electrons-holes are separated and transferred to the surface of semiconductor. These electrons-holes may recombine producing phonons and heat, leading to the decreased number of charge carries and ultimately less efficient photocatalysis. This step can be prevented by development of binary and ternary composites of visible light photocatalyst such as BiOI/BiOBr [43] and g-C_3N_4/Bi/BiOBr [86]. Binary and ternary heterojunctions enhance the photocatalysis rate by narrowing the band gap and suppressing electron-hole pair's recombination rate. In photocatalytic reaction, electrons and holes are generated when light strikes on the surface of photocatalyst. The major function of photo generated electrons is to reduce contaminants in wastewater and to react with oxygen to produce highly reactive superoxide radicals ($\bullet O_2^{-2}$); in the same process, when these electrons react with water molecules present in the environment, they produce highly reactive hydroxyl radicals and they are used in further enhancement of the pollutant degradation process. The radical species react with organic contaminants and convert them into simple less toxic molecules, with expected final degradation products such as CO_2 and H_2O. On the other hand, photo generated holes react with water molecules to produce hydroxyl radicals that react with contaminants and convert them into simple molecules. Photogenerated holes also react directly with pollutants such as methylene blue dyes and convert them into carbon dioxide and water directly, photocatalytic mechanism has been further elaborated in excellent reviews referenced here [87–89]. Another factor that can influence photocatalysis rate is the adsorption of pollutant material on the photocatalyst surface, as this process can increase the charge movement and enhance rate of redox reaction [26,90]. The high rate of charges recombination and broad gap of photocatalyst render photocatalyst incapable of working at higher scale. Various strategies are employed to overcome these limitations and the formation of heterojunction is one of them. For visible light photocatalyst BiOBr based binary and ternary composites are promising photocatalysts for wastewater treatment at higher level without compromising efficiency. For instance, ternary composite heterojunction PANI/BiOBr/$ZnFe_2O_4$ has been used to degrade of organic pollutants such as benzene through photocatalysis, as shown in Fig. 4 [72].

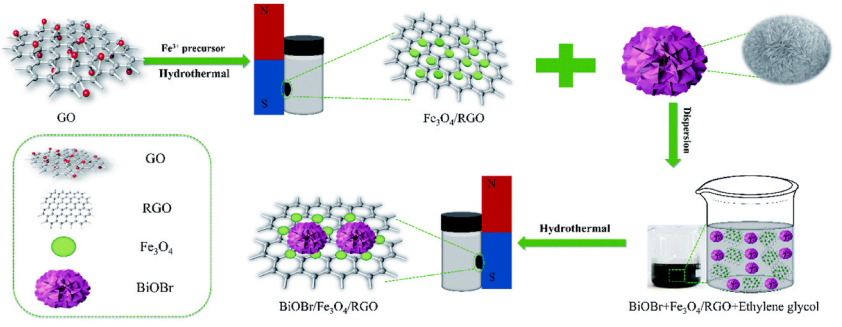

Fig. 3. Schematic illustration of BiOBr/Fe_3O_4/r-GO by hydrothermal method. Graphine oxide reacted with iron precursor to produce Fe_3O_4/r-GO which is then dipersed in ethylene glycol to produce ternary composite. Reproduced from Ref. [62] with permission from the Royal Society of Chemistry. This is an Open Access Article licensed under Creative Commons Attribution-Non Commercial 3.0 Unported Licence. https://creativecommons.org/licenses/by-nc/3.0/.

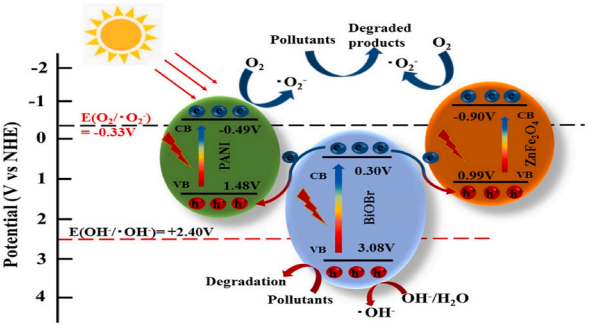

Fig. 4. Photocatalytic degradation mechanism of nitrobenzene by PANI/BiOBr/$ZnFe_2O_4$ Reproduced from Ref. [72] with permission from Elsevier. License Number: 5524161276243.

4. Strategies for enhancement of photocatalytic activity

4.1. Photosensitization

Photosensitization is a process of associating sensitizer with a photocatalyst to significantly enhance photocatalytic activity. A photosensitizer is a chemical specie that facilitates absorption of sunlight energy from ultraviolet to visible region and transfers this energy to a photocatalyst to initiate a reaction, degradation reaction in this case. It acts as an additional energy source for photocatalyst to drive a degradation reaction. Photosensitizers based on transition metals are widely used in diverse fields and they have coordinated complex with conjugated ligands [91]. Basically, photosensitizer enhance the sunlight absorption of photocatalyst by extending its absorption spectrum from UV light to visible region by employing chemi-sorbing or physico-sorbing substances. The photosensitization mechanism involves the transfer of visible light excited electron to the conduction band from the valence band of photocatalyst, where these electrons are used to progress the photocatalytic reaction. Owing to photostability and excellent photosensitizing properties, photosensitizers based on organometallic complex are widely used, the examples include ruthenium complexes, copper complexes and zinc complexes [92–95]. Aimed at wastewater treatment, degradation of phenols and orange II dye has been performed on Cu-Phthalocyanine (Cu-*Pc*) sensitized BiOBr/rGO under simulated sunlight. The result showed that loading of 0.25% of photosensitizer onto the photocatalyst surface gave significantly better results as compared to unloaded [51,96]. There are a large number of conjugated ligands that make porphyrins capable of absorbing a wide range in visible regions and owing to this feature, its complexes with transition metals are excellent photosensitizers for photocatalytic process. Photosensitization of BiOBr/BiOCl/PANI with Sn-porphyrin (Sn-PP) results in excellent photodegradation of methyl orange, with 96% degradation efficiency in only 10 min. Sn-PP sensitized BiOBr/BiOCl/PANI showed 7% more degradation efficiency than unloaded photocatalyst and this enhanced activity is due to the small band gap of Sn-PP and resultant more absorption in the visible region [97]. Photosensitization process can only extend the absorption spectrum of photocatalyst and it has limited use because it cannot narrow down the band gap or reduce charged recombination, and also they are expensive to use, and their performance is lower than the composite materials.

4.2. Facet control

Facet of crystalline photocatalyst is an important feature that can change the absorption of sunlight, geometry, electronic structure, surface physiochemical properties and intrinsic activity. To enhance the photocatalytic properties of semiconductor material, facet

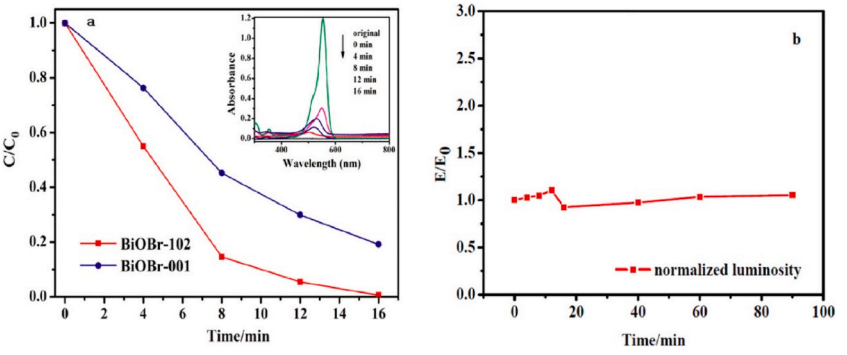

Fig. 5. (a) Residual concentration of dye for two facets of BiOBr, inset shows UV–Vis spectra of dye in aqueous solution changing with irradiation time, and (b) change in normalized luminosity with time. Reproduced with permission from the Ref. [107]. Copyright © 2014, American Chemical Society.

engineering has been in focus recently [98–101]. Different studies reported about four mechanisms that are followed in enhancement of photocatalytic activity through facet engineering.

1) Adsorption and activation of molecules caused by atomic re-arrangement in surface area and through this selectivity, catalytic activity is tuned [102,103].
2) Redox capabilities of electron-hole pairs are tuned by changing electric band structures through face engineering, resulting in better efficiency of photocatalyst [104].
3) Crystal orientation determines separation and transfer of their photoinduced charged carriers, leading to variation in charged density on surface reactions [105].
4) Spatial charge separation results in accumulation of photo generated electron-hole pairs at different facets and this can be achieved through facet control [106]. Zhang et al. synthesized (001) and (102) in BiOBr nanosheets through hydrothermal route and investigated their photocatalytic properties for environmental applications such as degradation of industrial dyes. The photocatalyst with (102) exposed facets successfully degraded the dye in 16 min of irradiation while (001) facet was slow to degrade, proving better efficiency of (102) exposed facets in BiOBr nanosheets. Fig. 5 presents a comparison of photocatalytic activity of both facets. Better photocatalytic performance by (102) is attributed to better band structure as it has higher valence band maximum and lower conduction band minimum and further more in (102) facet electron ejection is more efficient, redox capability of photoinduced charge is higher and it has narrowband gap (1.44eV) than (001) facets (2.22eV) [107].

In a similar process, lamellas of BiOBr sheets having a thickness range of 9–32 nm with (001) exposed facet were synthesized through a simple hydrolysis system and to achieve desired properties, temperature and solvent conditions were tuned. To make this synthesis easy and greener, no capping agent or surfactant was used. As a result, the active surface area of the photocatalyst was enhanced from 83% to 94% and this increased active surface areas was confirmed by enhancement in photocatalytic performance in degradation of rhodamine dye. This increase in photocatalytic activity is due to increased adsorption of dyes on the active surface of the photocatalyst [108]. Facet controlled photocatalytic materials are far from practical application owing to their difficult and harsh conditions requiring synthesis, use of expensive and toxic surfactants and multiple issues in their up scaling. There are limited methods of synthesis of facet controlled photocatalyst and shortcomings of characterization techniques are not adequate for detailed study of charge kinetics at facet surface.

4.3. Defect engineering

Recently, defect engineering in semiconductor photocatalysis has been focused owing to the ability of this technique to modulate charge separation, charge density, surface microstructure and electronic structure. Even coordination structure can be changed by introduction of an appropriate defect in semiconductor photocatalyst [109–111]. Owing to easiness in creation and prevalence in oxide materials, oxygen vacancies are the most studied defects in photocatalyst. Photogenerated electrons can stay on oxygen vacancy on the surface of photocatalyst, and it results in reducing recombination of charges. Oxygen vacancies increase adsorption of substrate and this adsorption enhances the rate of electron transfer due to coupling effect. Both these factors are highly beneficial for the overall photocatalytic process [112,113]. There are limited studies in which metal vacancies have been created to improve photocatalytic activity due to the absence of credible process and difficulty in operation of metal defects. However, Wang et al. synthesized BiOBr with oxygen defect through solvothermal method as a case study to portray defect engineered photocatalyst as an ideal procedure for environmental remediation. Oxygen rich photocatalyst was employed for degradation of 4-chlorophenol and results showed 10.9 times better efficiency of defect engineered photocatalyst as compared to simple BiOBr photocatalyst. This better photocatalytic property is ascribed to higher capturing capability in the visible region of light and high charge separation due to solid solutions and its synergistic effect with oxygen vacancy as they can narrow down band gap and impedes charge recombination [114]. Oxygen based vacancies are easy to create, but they require a synergizing factor through doping or doping to act as an efficient photocatalyst. There are several studies reporting oxygen vacancy created in bismuth oxybromide aimed at enhancement of photocatalytic activity for a variety of purposes such as degradation of pollutants and ammonia synthesis [115,116]. Bismuth based vacancies are rare case, for instance, Di et al. synthesized BiOBr with bismuth vacancy through ionic liquid assisted technique at room temperature. Defect engineered photocatalyst showed 3.8 times higher photocatalytic performance as compared to simple BiOBr photocatalyst. This enhanced activity of BiOBr ultrathin nanosheets with bismuth vacancy is due to more suitable electronic structure and improved interaction of the substrate with its surface [117]. To get benefit from the synergistic effect of metal and oxygen vacancy, Bi_3O_4Br nanosheets with bismuth defects has also been reported. The synergistic effect of two vacancies has been employed to increase the electron-hole separation through tuning of electronic structure and atomic arrangement. Resultant photocatalyst with double vacancy showed 30 times greater photocatalytic activity than simple photocatalyst [111]. Major limitations of defect engineering are harsh synthetic conditions and difficulty to industrialize.

4.4. Elemental doping

Doping is a widely reported phenomenon aimed at enhancement of photocatalytic properties of BiOBr photocatalyst. Doping inhibits electron-hole recombination, enhances visible light absorption and redox capability of photoexcited charge carriers [118]. It is necessary to add appropriate amount of dopant because excess amount of dopant can be sited for recombination of photo generated charges as demonstrated by Song et al. excess amount of zinc ion (Zn^{2+}) as dopant on BiOBr results in decreased photocatalytic activity

[119]. Dopant must have capability of electron/hole capture and should facilitate their separation and easy release towards surface migration for reaction initiation [120]. In most studies, rare earth metals, noble metals and transition metals have been used in cationic doping of BiOBr. Palladium is one of the noble metals that have been used as dopant in hydrothermally synthesized BiOBr by Meng et al. employing photodeposition method, as illustrated in Fig. 6. There was no covalent bonding between Pd and BiOBr, the dopant was only surface dispersed on the photocatalyst. Pd loaded photocatalyst was used to degrade phenol, and it degraded 100% while pristine BiOBr was able to degrade only 67%. Noble metal dopant enhance photocatalytic activity of semiconductor photocatalyst by two mechanisms; 1) enhancement of visible light absorption through surface Plasmon effect and 2) inhibition of photoexcited electron/hole pairs recombination [121]. The synthesis process of doped-photocatalyst also influences the photocatalytic activity, for instance, Pd doped BiOBr was synthesized through one pot facile synthesis but their activity was not good as compared to the aforementioned method. Incomplete reduction of Pd^{+2} to Pd NPs and non-uniform dispersion of dopant are two limitation of one pot facile synthesis that results in less photocatalytic activity [122]. Other noble metals employed for doping of BiOBr are silver, rhodium, platinum and gold [123–125].

Among rare earth metals, erbium (Er), yttrium (Y), cerium (Ce) and lanthanum (La) have been employed as dopant for BiOBr for photocatalytic degradation of environmental pollutants such as ciprofloxacin and rhodamine B [53,126]. Appropriate amount of dopant is an essential factor in rare earth metals doping, for instance, Imam et al. synthesized BiOBr through chemical precipitation method with 1,3 and 5% doping of La^{+3} and employed them for degradation of ciprofloxacin. Maximum degradation was exhibited by 3% Y–BiOBr was 87.6% degradation of wastewater contaminant as compared to pristine BiOBr which was 71.7% only. Increase in photocatalytic activity till 3% Y–BiOBr is ascribed to the increased surface area, from 19.65 m^2/g for pristine to 31.2 m^2/g, improved electron/hole separation and enhanced absorption and in 5% recombination sites for electron/hole are formed that results in decrease of photocatalytic activity [53]. Similarly, Er–BiOBr has also been reported with varying amount (1, 3, 5 and 8%) of Er and increases photocatalytic activity was observed till 3% and then decreased which is attributed to formation of electron/holes recombination centers [126].

Widely studied transition metal doping increases the life span of charged carriers by inhibiting their recombination through tuning band structure as in the case of Zn-doped BiOBr [119]. Some studies also reported that transition metal doping enhances the visible light absorption, for instance, Liu et al. synthesized trivalent iron (Fe^{3+}) doped BiOBr and studied their photocatalytic activity by degradation of methyl orange. Doped photocatalyst showed better degradation as compared to pristine BiOBr attributed to the increased absorption in the visible region of light and rapid electron/hole transfer [128]. Other transition metals employed for doping of BiOBr include titanium(Ti), copper (Cu), cobalt (Co), manganese (Mn) and niobium (Nb) [129–132]. There are limited number of studies that report anionic doping BiOBr. In a similar example of anionic dopant introduction, monovalent iodine anion was doped on BiOBr produced by precipitation method and employed for sunlight driven degradation of methyl orange. Iodine doped BiOBr showed more degradation of wastewater pollutant than pristine photocatalyst and this increase in photocatalytic activity is attributed to more electron/holes generation and broadening of light absorption from ultraviolet to visible region. This broadening of light absorption occurred due to decrease in band of gaps from 2.77 eV for pristine to 1.93 for iodine doped photocatalyst (Fig. 7) [127]. Noble metals are expensive and this render their doping an expensive procedure and not suitable for large scale applications. There is no single doping element that can increase surface area, narrowband gap, enhance charge separation and transfer, inhibits charge recombination and cost-effective. Other than these limitations of elemental doping necessity of appropriate amount of dopant is another issue.

4.5. Bismuth rich strategy

Band structure, particularly position of conduction band, is important for photocatalytic activity of semiconductor and this property is restricted by positive position of CB. Reactivity of electrons, that react with water to produce reacting radicals, is directly proportional to the negative position of CB, more negative position of CB more potent reducing electrons and vice versa. Density

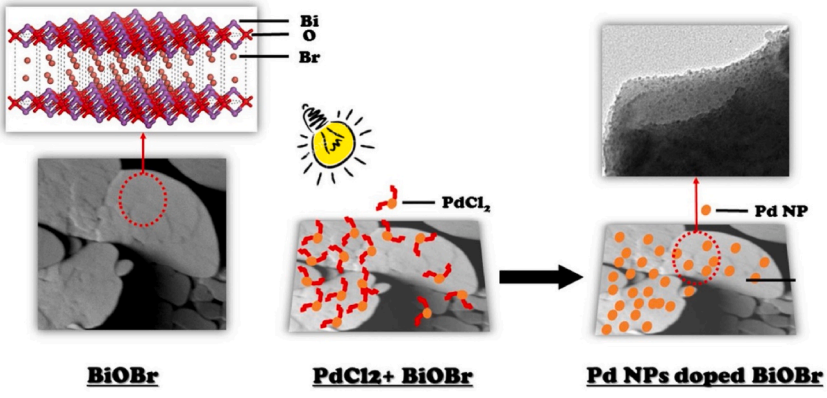

Fig. 6. Photodepostion of palladium nanoparticle on the surface of BiOBr. Reproduced from Ref. [121] with permission from Elsevier. License Number: 5524160508282.

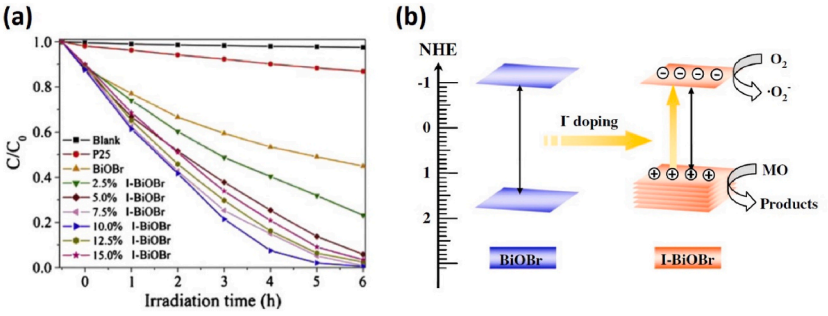

Fig. 7. (a) Comparison of photocatlaytic activity of various I–BiOBr and pristine BiOBr, (b) proposed band gap structures for photocatalytic removal of methyl orange (MO) using I–BiOBr and pristine BiOBr. Reproduced from the Ref. [127] with permission from Elsevier. License Number: 5524351242852. (For interpretation of the references to colour in this figure legend, the reader is referred to the Web version of this article.)

functional theory (DFT) suggests that the valence bond in BiOBr is primarily based on hybridization of 2p orbital of oxygen and 4p orbital of bromine while 6p orbital of bismuth gives rise to the valence band [133–136]. There are several studies which revealed that increase in bismuth content in BiOBr semiconductor enhances the photocatalytic performance. For instance, Mi et al. synthesized belt-like $Bi_4O_5Br_2$ nanomaterials through one step hydrolysis method at varying temperature and employed them in photocatalytic degradation of salicylic acid and resorcinol. Belt like $Bi_4O_5Br_2$ (B-25) synthesized at 25 °C showed 97% resorcinol degradation after 8 h and 95% salicylic acid degradation after 4 h and it was 50% higher than simple BiOBr. This enhanced photocatalytic property is due to increased surface area, narrower band gap and more negative CB of $Bi_4O_5Br_2$ (B-25) as shown in Fig. 8. Belt like $Bi_4O_5Br_2$ (B-25) has more negative CB ($E_{CB} = -0.37$) than plate like $Bi_4O_5Br_2$ ($E_{CB} = -0.34$) and BiOBr ($E_{CB} = -0.23$) and band gap narrow downed to 2.28 eV from 2.67 eV [54]. In similar studies, various bismuth rich oxybromides have been reported including $Bi_4O_5Br_2$ [137–140], Bi_5O_7Br [141,142], Bi_3O_4Br [143], $Bi_{12}O_{17}Br_2$ [144], $Bi_{24}O_{31}Br_{10}$ [127,145] and employed for environmental remediation like wastewater treatment. Synthesis of bismuth rich oxybromide is an ideal technique for optimization of band gap and band structure but it is difficult process to control amount of bismuth during synthesis. These developments are still far from practical applications to achieve highly efficient bismuth rich oxybromide photocatalyst for large scale application such as wastewater treatment, there is need for surface modification, better morphological control and tuning of internal electric field.

4.6. *Composite formation*

Heterojunctions are constructed through binary and ternary composite formation aimed at enhancement of photocatalytic activity. In these composites, there is heterojunction at the interface of two different semiconductors with suitable band gap and band structure that inhibits photoinduced electron/holes recombination. The need of composite formation arose due to inefficiency of single BiOBr photocatalyst in practical applications at industrial scale. Several studies proved that composite formation is an effective way to increase photocatalytic activity and this increase is due to its better visible light harvesting, more charges separation, layered structure endowed high surface area and ideal band structure for deep redox potential [146,147]. For instance, Hu et al. synthesized p-n heterojunction forming $BiOBr/Bi_2WO_6$ composite through solvothermal method and employed them for photocatalytic degradation of industrial dyes and phenolic compounds in wastewater. Photocatalytic degradation efficiency of composites was investigated by its employment in degradation of phenol and methylene blue and it was able to degrade 96% of methylene blue relative to BiOBr with degradation of 43% and Bi_2WO_6 with degradation of 62%. This increase in photocatalytic activity was the result of p-n junction formation that enhanced the separation and rapid transfer of photogenerated electron/holes pair [148]. Morphology of structure is an

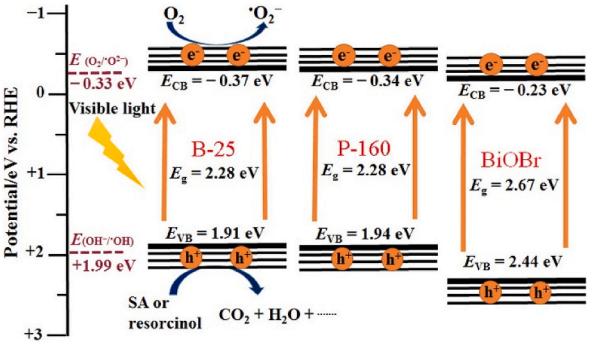

Fig. 8. The comparison of energy band structures of belt like $Bi_4O_5Br_2$ (B-25) synthesized at 25 °C, plate like $Bi_4O_5Br_2$ (P-160) synthesized at 260 °C and pristine BiOBr. Reproduced from the Ref. [54] with permission from Elsevier. License Number: 5524180360831.

important factor for photocatalytic activity. For instance, Rashid et al. synthesized butterfly cluster like lamellar BiOBr/TiO_2 binary composite through *in situ* deposition method at room temperature and employed them for photocatalytic breakdown of ciprofloxacin. Light absorption was increased owing to increased surface area up to 160.797 from 124.6 m^2/g due to butterfly cluster morphology of BiOBr (See Fig. 9). To determine suitability of the product for pharmaceutical wastewater treatment it was employed for the photocatalytic breakdown of 25 mg/L aqueous solution of ciprofloxacin under direct sunlight and marvelously 100% degradation was observed. Binary composites showed 5.2 and 9.4 times more photocatalytic activity than pristine BiOBr and TiO_2. Content percentage of BiOBr in binary composites was another factor that determined degradation rate and percentage of photocatalyst, highest photocatalytic activity was showed by 15% BiOBr/TiO_2 and it was more than binary composite containing 10%, 20%, 5% and pristine BiOBr. Other than surface area, inhibition of electron/holes recombination was another factor that enhanced photocatalytic activity of binary composite in such a way that TiO_2 acted as an electron sink and holes in BiOBr initiated the reaction of ciprofloxacin degradation [149].

Photocatalytic activity obtained for binary composites is still far from practical use owing to loss of activity during multiple cycle, chemical instability in the industrial environment and difficult photocatalyst recovery process. For advancement of photocatalytic properties of binary composites three methods are employed including doping [64], photosensitization [51] and formation of ternary composites [61]. In case of binary composites of BiOBr doping and photosensitization could not produce desired result with limitations due to expensive cost of dopant and sensitizers. However, ternary composites proved to be promising candidates in fulfilling the requirement of an ideal photocatalyst for wastewater treatment at industrial level. Formation of ternary composites has solved the problem of photocatalyst recovery by introducing magnetic ternary composites. For instance, Li and co-workers reported synthesis of Fe_3O_4/BiOBr/BiOI based ternary composite photocatalyst by solvothermal route to degrade rhodamine B, a textile wastewater dye. The ternary composite exhibited 100% degradation of dye in 80 min., showing superior photocatalytic activity to the Fe_3O_4/BiOBr binary composite. This increase in photocatalytic activity was due to better light absorption owing to more suitable band gap and band structure. In ternary composites, synthetic method greatly influences the surface area of the photocatalyst and ultimately photocatalytic activity, for example, solvothermally synthesized Fe_3O_4/BiOBr/BiOI has more active surface area (48.30 m^2/g) than that of a similar composite synthesized by co-precipitation method [50]. Ternary composites offer improved light absorption, high quantum yield, rapid electron transfer and better photocatalytic activity. For instance, Zhang et al. synthesized PANI/BiOBr/$ZnFe_2O_4$ and tried to harness high charge carrier mobility and environmental stability of the conducting polymer polyaniline (PANI) for photocatalytic treatment of textile wastewater. The synthesized ternary composite completely degraded the rhodamine B dye in 30 min. Ternary composite showed better photocatalytic performance as compared to the binary composite and individual components and its enhancement is attributed to the increased charge carriers generation and their rapid transfer and separation. To assess the wide applicability of PANI/BiOBr/$ZnFe_2O_4$ ternary composite, it was used for photocatalytic removal of various other organic pollutants such as norfloxacin, methylene blue, bisphenol A and methyl orange with removal rates of 89.7%, 90.97%, 75.64% and 95.32%, respectively, and after 60 min visible irradiation recorded. The effect of pH on photocatalytic activity of photocatalyst was also studied and reportedly PANI/BiOBr/$ZnFe_2O_4$ ternary composite showed higher photocatalytic activity at neutral pH = 7. In alkaline solution, degradation efficiency was enhanced due to the increased interaction of photocatalyst and dye owing to negative charge of BiOBr and positive charge on rhodamine B. Acidic conditions decreased photocatalytic performance of ternary composite and this decrease was due to positive charge on BiOBr resulting in electrostatic repulsion and less interaction. For practical applications, other than chemical stability, photostability and reusability are crucial. To determine reusability, ternary composite was used to degrade rhodamine B

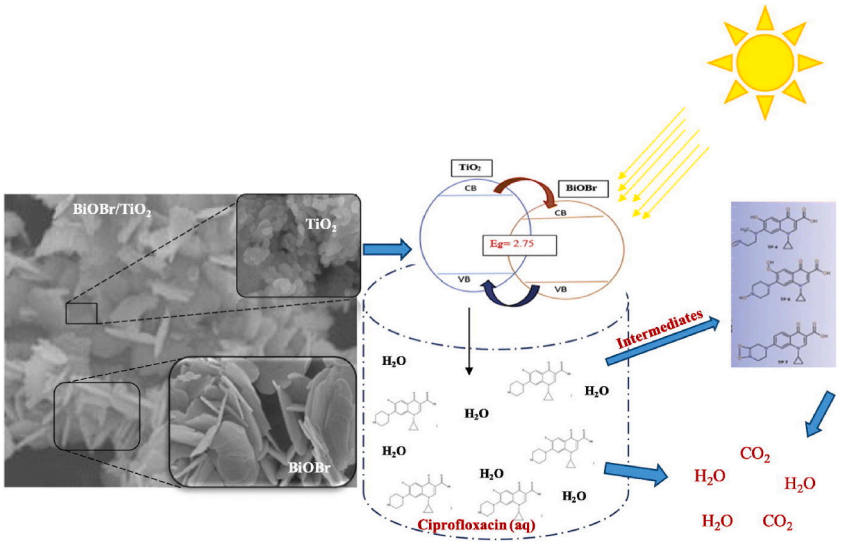

Fig. 9. Increased surface area of binary composites due to butter cluster like morphology and subsequent photocatalytic degradation mechanism. Reproduced from Ref. [149] with permission from Elsevier. License Number: 5524190077045.

Table 1
BiOBr based binary and ternary composite for wastewater treatment and their photodegradation percentage with degraded pollutant.

Sr. No.	Composite	Band gap	Pollutant	Photodegradation (%)		Ref.
				BiOBr	Composite	
1.	$BiOBr/TiO_2$	2.76 eV	Ciprofloxacin	30.7	100	[149]
2.	$BiOBr/TiO_2$	2.88 eV	Rhodamine B	78	92.8	[78]
3.	$BiOBr/TiO_2$	–	Methyl orange	40	91	[154]
4.	$BiOBr/TiO_2$	2.79 eV	Rhodamine B	70	100	[152]
6.	$NiFe_2O_4/BiOBr$	–	Rhodamine B	46	96	[158]
7.	BiOBr/RGO	–	Methylene blue	53.5	94.7	[159]
8.	BiOBr/RG	2.58 eV	Rhodamine B	50	100	[160]
9.	$CdWO_4/BiOBr$	–	Rhodamine B	40	100	[161]
10.	$BiPO_4/BiOBr$	2.77 eV	Dichlorobenzene	26.8	53.6	[162]
11.	$BiOBr/BiPO_4$	2.7 eV	Methylene blue	40	96	[163]
12.	$CdWO_4/BiOBr$	–	Rhodamine B	40	100	[161]
13.	$BiOBr/Bi_2WO_6$	2.6 eV	Methylene blue	43	96	[148]
14.	Ag/BiOBr	2.88 eV	Rhodamine B	50	100	[164]
15.	$BiOBr/Bi_4O_5Br_2$	2.43 eV	Ciprofloxacin	50	91	[165]
16.	$BiOBr/Bi_4O_5Br_2$	–	Ciprofloxacin	40	94	[166]
17.	$BiOBr/Bi_2O_2CO_3$	2.82 eV	Rhodamine B	46.99	92.83	[74]
18.	$BiVO_4/BiOBr$	2.75 eV	Rhodamine B	60	95	[158]
21.	BiOBr/CdS	2.48 eV	Bisphenol A	42	78	[167]
24.	$BiPO_4/BiOBr$	2.63 eV	Rhodamine B	57	98	[76]
25.	$BiPO_4/BiOBr$	2.78 eV	Rhodamine B	71.3	98	[168]
26.	$BiOBr/Bi_2SiO_5$	2.61 eV	Tetracycline	70	96.1	[169]
27.	$BiOBr/Bi_{12}O_{17}Cl_2$	2.4 eV	Methyl orange	70	92	[170]
28.	$SnO_2/BiOBr$	2.80 eV	Rhodamine B	60	98.2	[171]
29.	$BiOBr/Ti_3C_2$	2.88 eV	Rhodamine B	79	100	[172]
30.	$BiOBr/Bi_2MoO_6$	2.77 eV	Ciprofloxacin	38.36	84.63	[173]
31.	$BiOBr/Bi_2S_3$	1.75 eV	Cr(IV)	15	100	[48]
32.	$Bi_2S_3/BiOBr$	2.25 eV	Methyl orange	48	60	[81]
33.	$Bi_2O_4/BiOBr$	–	Methyl orange	15	100	[174]
34.	$WS_2/BiOBr$	2.12 eV	Ciprofloxacin	61	92	[175]
35.	Ag QDs/BiOBr	–	Rhodamine B	32.3	83.8	[176]
36.	$C_3N_4/BiOBr$	–	Rhodamine B	65	100	[177]
37.	α-$Fe_2O_3/BiOBr$	1.90 eV	Rhodamine B	60	95	[178]
38.	BiOBr/BHO	–	Rhodamine B	75	100	[179]
39.	$Bi_2MoO_6/BiOBr$	–	Methylene blue	20	90	[180]
40.	CQDs/BiOBr	–	Rhodamine B	22.8	95.8	[181]
41.	$LaFeO_3/BiOBr$	–	Rhodamine B	95.2	95.8	[182]
42.	BP/BiOBr	2.75 eV	Tetracycline	25	85	[183]
43.	$BiOBr/NaBiO_3$	2.7 eV	Chlorophenol	0.8	92	[150]
44.	BiOBr/ZnO	2.66 eV	Methylene blue	42	90	[184]
45.	CoS/BiOBr	–	Glyphosate	21.9	74.7	[185]
46.	$BiOBr/SrFe_{12}O_{19}$	2.69 eV	Rhodamine B	86	97	[186]
47.	$LaVO_4/BiOBr$	2.57 eV	acetone	36.1	94.5	[187]
48.	MWCNT/BiOBr	2.86 eV	Rhodamine B	70	97	[188]
49.	$Zn_2SnO_4/BiOBr$	2.88 eV	Rhodamine B	69	96	[189]
52.	ZnS/BiOBr	2.69 eV	Tetracycline	70	82	[182]
54.	$BiOBr/Ag_6Si_2O_7$	2.41 eV	Methylene blue	25	98	[190]
55.	BiOBr/BiOI	2.64 eV	Rhodamine B	20.8	98.6	[54]
56.	BiOBr/BiOI	–	Tetracycline hydrochloride	33	53	[49]
58.	BiOI/BiOBr	2.18 eV	Rhodamine B	47.1	71	[146]
59.	$Bi_4O_5Br_2/BiOI$	1.68 eV	Crystal violet	20	99	[68]
60.	I–BiOCl/I–BiOBr	2.18 eV	Methyl orange	45	95	[147]
61.	$Bi_3O_4Cl/Bi_{24}O_{31}Br_{10}$	2.73 eV	Crystal violet	–	99	[80]
62.	BiOCl/BiOBr	–	Methylene blue	72	93	[191]
63	BiOBr/UiO-66	2.80	Atrazine	44	88	[192]
64	$BiOBr/La_2Ti_2O_7$	3.4	Rhodamine B	80	100	[193]
65	BiOBr/TP	3.0	Rhodamine B	–	100	[194]
66.	$PANI/BiOBr/ZnFe_2O_4$	–	Rhodamine B	60	99.26	[72]
67.	$Fe_3O_4/BiOBr/BiOI$	1.77 eV	Rhodamine B	20.8	99.8	[50]
68.	SiO_2/PDA/BiOBr	2.68 eV	Rhodamine B	75	100	[195]
69.	$AgBr/g\text{-}C_3N_4/BiOBr$	2.82 eV	Rhodamine B	50	98	[75]
70.	K/g-C3N4/BiOBr	2.66 eV	Rhodamine B	75	99	[64]
71.	$g\text{-}C_3N_4/BiOI/BiOBr$	–	Methylene blue	40	80	[156]
72.	$g\text{-}C_3N_4/BiOI/BiOBr$	–	Methyl orange	43.5	99.7	[155]
73.	$g\text{-}C_3N_4$/Bi/BiOBr	2.43 eV	Rhodamine B	52	98	[86]
74.	Ag/BiOBr/GO	2.76 eV	Rhodamine B	50	98	[66]
75.	Bi/BiOBr/AgBr	–	Rhodamine B	48.4	95.6	[65]
76.	$Fe_3O_4/mSiO_2/BiOBr$	–	Methylene blue	2.58	51.27	[69]

(*continued on next page*)

Table 1 (*continued*)

Sr. No.	Composite	Band gap	Pollutant	Photodegradation (%)		Ref.
				BiOBr	Composite	
77.	$BiOBr/Fe_3O_4/RGO$	2.38 eV	Rhodamine B	63	96	[62]
78.	BiOBr/BiOCl/PANI	2.2 eV	Methyl orange	38	89	[77]
79.	$BiOBr/TiO_2/G$	–	Rhodamine B	–	100	[153]
80.	BiVO4/BiOBr/Pd	2.48 eV	Rhodamine B	45	100	[196]
81.	$rGO/Bi_2S_3/BiOBr$	1.49 eV	Cr(IV)	55	95	[197]
82.	$Bi_{12}O_{17}C_{l2}/Bi_3O_4Br/Bi_4O_5I_2$	2.43 eV	Crystal violet	–	99.9	[56]
83.	$TiO_2/BiOBr/Bi_2S_3$	2.55 eV	2,4-Dichlorophenoxyacetic acid	22	98	[198]
84.	$Ag_2CO_3/BiOBr/CdS$	–	Tetracycline	80	98.79	[199]
85.	$Fe_3O_4/BiOBr/CQDs$	1.31 eV	Carbamazepine	68.89	99.52	[151]
86.	$Bi_2WO_6/BiOBr/RGO$	2.4 eV	Ciprofloxacin	45.3	90.7	[200]
87.	$Fe_3O_4/LDO/BiOBr$	1.80 eV	Cr(IV)	45	98	[201]
88.	$FeVO_4/Bi_4O_5Br_2/BiOBr$	–	Cr(IV)	14	96	[202]

three time and only trivial 1.4% decrease in photocatalytic activity was recorded as compared to BiOBr where this decrease was significant 10% for three cycle. X-ray diffraction (XRD) pattern of $PANI/BiOBr/ZnFe_2O_4$ after three cycles of its usage showed lack of differences, thus indicating its high photostability [72]. Conclusively binary and ternary composites of BiOBr are the most optimized and promising candidates for photocatalytic wastewater treatment owing to their highest optimization in terms of band gap, band structure, recovery, reusability, photostability, chemical stability and quantum yield. In subsequent paragraphs, we will discuss the application of BiOBr based binary ad ternary composite for wastewater treatment.

5. Application of BiOBr based binary and ternary composites in wastewater treatment

A literature on the application of BiOBr based binary and ternary composites in wastewater treatment is widely available. This section aims to deliberate the mechanism of photocatalytic activity enhancement through formation of binary and ternary composites. Table 1 clearly demonstrates that binary and ternary composite results in better degradation of wastewater pollutants compared to BiOBr. The average increase in degradation percentage is more than 50%, for instance in the case of $BiOBr/NaBiO_3$, chlorophenol degradation percentage was increased from 0.8% (BiOBr) to more than 92% with quantum yield of about 0.365. Multiple factors are involved in this enhancement of photocatalytic activity, including band gap, band structure, and interface. Modulation of band gap is the leading factor that is contributing mainly towards enhanced efficiency, by formation of binary composite band gap was optimally narrowed down from its component. Band gap of $NaBiO_3$ is 2.60 eV and that of BiOBr is 2.88 eV while after formation of binary composite it is reduced to 2.52 eV which is optimum in terms of both efficient sunlight harvesting and charge carrier generation. Valence band is based in BiOBr and its amount is important for generation of suitable band structure for maximum photocatalytic activity, in this case, 9% BiOBr is ideal for highest photocatalytic efficiency, increase results in change in band structure and reduction of photocatalytic activity. Significance of the interface was determined by comparing photocatalytic activity of 9% $BiOBr/NaBiO_3$ mechanical mixture which gave only 72% photodegradation efficiency, about 20% less than original catalyst. In composite form two interfaces were closely coupled that reduce electron and hole recombination while in case of mechanical mixture there is no influence of interface in reducing charge recombination. Conclusively, binary composite results in efficient visible light harvesting due to modulated band gap, rapid separation with high redox potential, interface to prevent recombination of electrons and holes and 9% amount of BiOBr to balance the redox ability and separation efficiency of photogenerated charges [150]. Synthesis of binary composites results in improved photocatalytic activity but developments are still far from practical applications. To harness the interfacial aspect of composites leading to enhanced surface area and increased charge separation, researchers have switched to the synthesis of ternary composites for wastewater treatment. For instance, Bi/BiOBr/AgBr has about two times greater photodegradation percentage against rhodamine B than pristine BiOBr which can only degrade 48% of wastewater pollutants while ternary composites easily degraded about 95% of the dye. This enhanced photocatalytic performance is ascribed to major three factors; high absorption capacity in the visible region, instant electron transfer and high charge separation efficiency. In this case, presence of Bi metallic nanoparticles results in surface plasmon resonance that cause more absorption in visible region. It has also been reported that higher visible light absorption is not only contributing factor towards enhanced photocatalytic activity of ternary composites, but also the smaller arc radius enhances charge separation efficiency and speed of electron transfer [65]. Recovery of catalyst from wastewater after degradation of target pollutant is a one of the still not solved challenges. Synthesis of magnetic ternary composites containing Fe_2O_3 makes it easier to recover the photocatalyst. Moreover, the presence of metal-oxygen bond is beneficial as it can enhance photocatalytic activity by increasing surface area and facilitating adsorption of pollutants, for example, $Fe_3O_4/BiOBr/BiOI$ [50], $Fe_3O_4/mSiO_2/BiOBr$ [69], $BiOBr/Fe_3O_4/RGO$ [62] and $Fe_3O_4/BiOBr/CQDs$ [151]. Irrespective of synthetic method, ternary composites are better than binary composites owing to ideally modulated band gap, more suitable band structure and more adsorption area for pollutants such as Bi/BiOBr/AgBr has better degradation efficacy than binary composites of its components and showed 4.9 and 1.4 times faster degradation of rhodamine B than BiOBr/AgBr and Bi/BiOBr, respectively [65]. Similarly, $BiOBr/TiO_2/G$ was found to be a better photocatalyst than $BiOBr/TiO_2$ prepared for variety of pollutant degradation [78,149,152–154] and $g\text{-}C_3N_4/BiOI/BiOBr$ can degrade different wastewater pollutants more efficiently than binary composites of its components such as BiOI/BiOBr [49,54,146,155–157]. Summarily, BiOBr based composites whether binary or ternary, are better photocatalyst for wastewater treatment than pure BiOBr.

These composites offer more visible light harvesting to the photocatalyst through narrowband gap, increased charge separation, reduced charge recombination by suitable band structures, and increased surface area for both enhanced absorption of sunlight and adsorption of target pollutant. Last but not the least, such photocatalysts can be easily recovered after photocatalytic action if magnetic components are employed in composites.

6. Current challenges

Though reported literature, it is evident that a significant development in the field of BiOBr based binary and ternary composites has been made. However, these developments are still far from practical applications. Composites result in increased surface active sites but their role in enhancing photocatalytic activity is undefined and cannot be manipulated positively. Immobilization of substrate on the surface of photocatalyst is one of the crucial steps; it needs to explored for better performance. In laboratory, it is easy to degrade model pollutant but real wastewater is complex mixture that demands more optimization in terms of selectivity and environmental conditions such pH, temperature and nature of wastewater. Reported photocatalysts are specialized for only single or a group of pollutants that is challenging to degrade real wastewater by a single photocatalyst. To employ BiOBr based composite photocatalysts at large scale for industrial wastewater, their manufacturing at commercial level is one of the major challenge that needs to be addressed. Conclusively, other than band gap; band structure, surface optimization, reusability, recovery and absence of solid supports are huge challenges.

7. Conclusion

Owing to the layered structure of BiOBr, their composites are efficient photocatalysts for wastewater treatment. For enhancement of photocatalytic activity, other techniques such as doping, facet control and defect engineering are available to form binary and ternary composites. In this review, recent literature was summarized to extract vital information for enhancement strategies for BiOBr based photocatalysts and primarily focusing on binary and ternary composite for photocatalytic wastewater treatment, while briefly outlining their synthesis methods. This information is substantial for researchers to move forward in application of these binary and ternary composites at industrial scale wastewater treatment. The synergistic effect of individual components in the composites along with other enhancement strategies can be beneficial for large scale applications. For efficient removal of pollutants from wastewater, we believe that future research should be focused on coupling photocatalytic process with complementing techniques such as membrane based technologies and anaerobic digestion. Therefore, more advanced research is expected in this field aimed at designing new composites having more suitable band gap, band structure, better chemical and physical stability and surface properties that could revolutionize photocatalytic wastewater treatment.

Declaration of competing interest

The authors declare that they have no known competing financial interests or personal relationships that could have appeared to influence the work reported in this paper.

Data availability

No data was used for the research described in the article.

References

[1] L. Han, et al., Photocatalytic degradation of mixed pollutants in aqueous wastewater using mesoporous 2D/2D TiO2 (B)-BiOBr heterojunction, J. Mater. Sci. Technol. 70 (2021) 176–184.
[2] D. Lu, et al., A facile one-pot synthesis of TiO2-based nanosheets loaded with MnxOy nanoparticles with enhanced visible light–driven photocatalytic performance for removal of Cr (VI) or RhB, Appl. Catal. B Environ. 179 (2015) 558–573.
[3] D. Kanakaraju, B.D. Glass, M. Oelgemöller, Titanium dioxide photocatalysis for pharmaceutical wastewater treatment, Environ. Chem. Lett. 12 (1) (2014) 27–47.
[4] N. Abdullah, et al., Recent trends of heavy metal removal from water/wastewater by membrane technologies, J. Ind. Eng. Chem. 76 (2019) 17–38.
[5] A. Singh, et al., Biological remediation technologies for dyes and heavy metals in wastewater treatment: new insight, Bioresour. Technol. 343 (2022), 126154.
[6] C.A. Martínez-Huitle, M. Panizza, Electrochemical oxidation of organic pollutants for wastewater treatment, Curr. Opin. Electrochem. 11 (2018) 62–71.
[7] A. Kumar, D. Pal, Antibiotic resistance and wastewater: correlation, impact and critical human health challenges, J. Environ. Chem. Eng. 6 (1) (2018) 52–58.
[8] Z. Honarmandrad, et al., Activated Persulfate and Peroxymonosulfate Based Advanced Oxidation Processes (AOPs) for Antibiotics Degradation–A Review, Water Resources and Industry, 2022, 100194.
[9] S. Martin, W. Griswold, Human health effects of heavy metals, Environ. Sci. Technol. briefs citizens 15 (2009) 1–6.
[10] B. Lellis, et al., Effects of textile dyes on health and the environment and bioremediation potential of living organisms, Biotechnol. Res. Innov. 3 (2) (2019) 275–290.
[11] E. Cako, et al., Ultrafast degradation of brilliant cresyl blue under hydrodynamic cavitation based advanced oxidation processes (AOPs), Water Resour. Ind. 24 (2020), 100134.
[12] F.A. Janjhi, et al., MXene-Based Materials for Removal of Antibiotics and Heavy Metals from Wastewater–A Review, Water Resources and Industry, 2023, 100202.
[13] U. Water, UN world water development report, Nat. based Solutions Water (2018), 2018.
[14] S.N. Ahmed, W. Haider, Heterogeneous photocatalysis and its potential applications in water and wastewater treatment: a review, Nanotechnology 29 (34) (2018), 342001.

[15] S. Suárez, et al., How are pharmaceutical and personal care products (PPCPs) removed from urban wastewaters? Rev. Environ. Sci. Biotechnol. 7 (2) (2008) 125–138.
[16] K. Fedorov, et al., Activated sodium percarbonate-ozone (SPC/O3) hybrid hydrodynamic cavitation system for advanced oxidation processes (AOPs) of 1, 4-dioxane in water, Chem. Eng. J. 456 (2023), 141027.
[17] Y. Zhang, S.-U. Geißen, C. Gal, Carbamazepine and diclofenac: removal in wastewater treatment plants and occurrence in water bodies, Chemosphere 73 (8) (2008) 1151–1161.
[18] E. Mousset, K. Doudrick, A review of electrochemical reduction processes to treat oxidized contaminants in water, Curr. Opin. Electrochem. 22 (2020) 221–227.
[19] M.A. Zazouli, L.R. Kalankesh, Removal of precursors and disinfection by-products (DBPs) by membrane filtration from water; a review, J./ Environ. Health Sci. Eng. 15 (1) (2017) 1–10.
[20] A. Azimi, et al., Removal of heavy metals from industrial wastewaters: a review, ChemBioEng Rev. 4 (1) (2017) 37–59.
[21] A. Zularisam, A. Ismail, R. Salim, Behaviours of natural organic matter in membrane filtration for surface water treatment—a review, Desalination 194 (1–3) (2006) 211–231.
[22] C. Yu, et al., Thermal stability, microstructure and photocatalytic activity of the bismuth oxybromide photocatalyst, Chin. J. Chem. 30 (3) (2012) 721–726.
[23] A. Fernandes, et al., Synergistic effect of TiO2 photocatalytic advanced oxidation processes in the treatment of refinery effluents, Chem. Eng. J. 391 (2020), 123488.
[24] O. Arar, et al., Various applications of electrodeionization (EDI) method for water treatment—a short review, Desalination 342 (2014) 16–22.
[25] Z. Li, X. Meng, Z. Zhang, Fewer-layer BN nanosheets-deposited on Bi2MoO6 microspheres with enhanced visible light-driven photocatalytic activity, Appl. Surf. Sci. 483 (2019) 572–580.
[26] S.R. Pouran, A.A. Aziz, W.M.A.W. Daud, Review on the main advances in photo-Fenton oxidation system for recalcitrant wastewaters, J. Ind. Eng. Chem. 21 (2015) 53–69.
[27] T. Esakkimuthu, D. Sivakumar, S. Akila, Application of nanoparticles in wastewater treatment, Pollut. Res. 33 (3) (2014) 567–571.
[28] S. Singh, et al., Applications of nanoparticles in wastewater treatment, in: Nanobiotechnology in Bioformulations, Springer, 2019, pp. 395–418.
[29] M. Sagir, et al., Nanoparticles and significance of photocatalytic nanoparticles in wastewater treatment: a review, Curr. Anal. Chem. 17 (1) (2021) 38–48.
[30] N.S.M. Shahrodin, et al., Superparamagnetic iron oxide as photocatalyst and adsorbent in wastewater treatment–a review, Micro Nanosyst. 12 (1) (2020) 4–22.
[31] A. Fernandes, et al., Integrated photocatalytic advanced oxidation system (TiO2/UV/O3/H2O2) for degradation of volatile organic compounds, Sep. Purif. Technol. 224 (2019) 1–14.
[32] J.A. Khan, et al., Synthesis of eosin modified TiO2 film with co-exposed {001} and {101} facets for photocatalytic degradation of para-aminobenzoic acid and solar H2 production, Appl. Catal. B Environ. 265 (2020), 118557.
[33] N.S. Shah, et al., Enhanced solar light photocatalytic performance of Fe-ZnO in the presence of H2O2, S2O82−, and HSO5− for degradation of chlorpyrifos from agricultural wastes: toxicities investigation, Chemosphere 287 (2022), 132331.
[34] V. Landge, et al., S-scheme heterojunction Bi2O3-ZnO/Bentonite clay composite with enhanced photocatalytic performance, Sustain. Energy Technol. Assessments 45 (2021), 101194.
[35] N.S. Shah, et al., Solar light driven degradation of norfloxacin using as-synthesized Bi3+ and Fe2+ co-doped ZnO with the addition of HSO5−: toxicities and degradation pathways investigation, Chem. Eng. J. 351 (2018) 841–855.
[36] S.R. Mishra, M. Ahmaruzzaman, Cerium oxide and its nanocomposites: structure, synthesis, and wastewater treatment applications, Mater. Today Commun. 28 (2021), 102562.
[37] B. Bethi, et al., Photocatalytic Decolourization of Rhodamine-B Dye by Visible Light Active ZIF-8/BiFeO3 Composite, Environmental Science and Pollution Research, 2022, pp. 1–14.
[38] P. Gao, et al., A critical review on bismuth oxyhalide based photocatalysis for pharmaceutical active compounds degradation: modifications, reactive sites, and challenges, J. Hazard Mater. 412 (2021), 125186.
[39] Z. Wang, et al., Multiply structural optimized strategies for bismuth oxyhalide photocatalysis and their environmental application, Chem. Eng. J. 374 (2019) 1025–1045.
[40] L. Ye, et al., Recent advances in BiOX (X= Cl, Br and I) photocatalysts: synthesis, modification, facet effects and mechanisms, Environ. Sci. J. Integr. Environ. Res.: Nano 1 (2) (2014) 90–112.
[41] D.S. Bhachu, et al., Bismuth oxyhalides: synthesis, structure and photoelectrochemical activity, Chem. Sci. 7 (8) (2016) 4832–4841.
[42] J. Chen, et al., The dominant {001} facet-dependent enhanced visible-light photoactivity of ultrathin BiOBr nanosheets, Phys. Chem. Chem. Phys. 16 (38) (2014) 20909–20914.
[43] J. Cao, et al., Novel BiOI/BiOBr heterojunction photocatalysts with enhanced visible light photocatalytic properties, Catal. Commun. 13 (1) (2011) 63–68.
[44] S.S. Imam, R. Adnan, N.H.M. Kaus, The photocatalytic potential of BiOBr for wastewater treatment: a mini-review, J. Environ. Chem. Eng. 9 (4) (2021), 105404.
[45] G. Tekin, G. Ersöz, S. Atalay, Visible light assisted Fenton oxidation of tartrazine using metal doped bismuth oxyhalides as novel photocatalysts, J. Environ. Manag. 228 (2018) 441–450.
[46] S.-l. Wang, et al., Moderate valence band of bismuth oxyhalides (BiOXs, X= Cl, Br, I) for the best photocatalytic degradation efficiency of MC-LR, Chem. Eng. J. 259 (2015) 410–416.
[47] L. Wu, et al., Mechanochemical syntheses of bismuth oxybromides BixOyBrz as visible-light responsive photocatalyts for the degradation of bisphenol A, J. Solid State Chem. 270 (2019) 458–462.
[48] Z. Long, et al., Preparation and application of BiOBr-Bi2S3 heterojunctions for efficient photocatalytic removal of Cr (VI), J. Hazard Mater. 407 (2021), 124394.
[49] X. Yang, et al., Construction of porous-hydrangea BiOBr/BiOI nn heterojunction with enhanced photodegradation of tetracycline hydrochloride under visible light, J. Alloys Compd. 864 (2021), 158784.
[50] J. Li, et al., Visible-light photocatalytic performance, recovery and degradation mechanism of ternary magnetic Fe 3 O 4/BiOBr/BiOI composite, RSC Adv. 9 (41) (2019) 23545–23553.
[51] S. Ouedraogo, et al., Bismuth oxybromide/reduced graphene oxide heterostructure sensitized with Zn-tetracarboxyphthalocyanine as a highly efficient photocatalyst for the degradation of Orange II and phenol, J. Environ. Chem. Eng. 10 (2) (2022), 107332.
[52] X.Y. Kong, et al., Topotactic transformation of bismuth oxybromide into bismuth tungstate: bandgap modulation of single-crystalline {001}-faceted nanosheets for enhanced photocatalytic CO2 reduction, ACS Appl. Mater. Interfaces 12 (24) (2020) 26991–27000.
[53] S.S. Imam, R. Adnan, N.H.M. Kaus, Influence of yttrium doping on the photocatalytic activity of bismuth oxybromide for ciprofloxacin degradation using indoor fluorescent light illumination, Res. Chem. Intermed. 44 (9) (2018) 5357–5376.
[54] Y. Mi, et al., Synthesis of belt-like bismuth-rich bismuth oxybromide hierarchical nanostructures with high photocatalytic activities, J. Colloid Interface Sci. 534 (2019) 301–311.
[55] F. Qiu, et al., In-situ synthesis of novel Z-scheme SnS2/BiOBr photocatalysts with superior photocatalytic efficiency under visible light, J. Colloid Interface Sci. 493 (2017) 1–9.
[56] C.-W. Siao, et al., Controlled hydrothermal synthesis of bismuth oxychloride/bismuth oxybromide/bismuth oxyiodide composites exhibiting visible-light photocatalytic degradation of 2-hydroxybenzoic acid and crystal violet, J. Colloid Interface Sci. 526 (2018) 322–336.
[57] F.-Y. Liu, et al., Lead bismuth oxybromide/graphene oxide: synthesis, characterization, and photocatalytic activity for removal of carbon dioxide, crystal violet dye, and 2-hydroxybenzoic acid, J. Colloid Interface Sci. 562 (2020) 112–124.
[58] C.-C. Chen, et al., Hydrothermal synthesis of BiOxBry/BiOmIn/GO composites with visible-light photocatalytic activity, J. Taiwan Inst. Chem. Eng. 133 (2022), 104272.

[59] N.B. Saber, et al., A review of ternary nanostructures based noble metal/semiconductor for environmental and renewable energy applications, J. Mater. Res. Technol. 9 (6) (2020) 15233–15262.
[60] C. Prasad, H. Tang, I. Bahadur, Graphitic carbon nitride based ternary nanocomposites: from synthesis to their applications in photocatalysis: a recent review, J. Mol. Liq. 281 (2019) 634–654.
[61] M. Arumugam, et al., Recent developments on bismuth oxyhalides (BiOX; X= Cl, Br, I) based ternary nanocomposite photocatalysts for environmental applications, Chemosphere 282 (2021), 131054.
[62] M. Zheng, et al., Novel recyclable BiOBr/Fe 3 O 4/RGO composites with remarkable visible-light photocatalytic activity, RSC Adv. 10 (34) (2020) 19961–19973.
[63] K.-Y. Shih, Y.-L. Kuan, E.-R. Wang, One-step microwave-assisted synthesis and visible-light photocatalytic activity enhancement of BiOBr/RGO nanocomposites for degradation of methylene blue, Materials 14 (16) (2021) 4577.
[64] J. Qu, et al., Visible-light-responsive K-doped g-C3N4/BiOBr hybrid photocatalyst with highly efficient degradation of Rhodamine B and tetracycline, Mater. Sci. Semicond. Process. 112 (2020), 105023.
[65] J. Lyu, Z. Li, M. Ge, Novel Bi/BiOBr/AgBr composite microspheres: ion exchange synthesis and photocatalytic performance, Solid State Sci. 80 (2018) 101–109.
[66] C. Li, et al., Performance of Ag/BiOBr/GO composite photocatalyst for visible-light-driven dye pollutants degradation, J. Mater. Res. Technol. 9 (1) (2020) 610–621.
[67] Y. Guo, et al., Fabrication of Ag/CDots/BiOBr ternary photocatalyst with enhanced visible-light driven photocatalytic activity for 4-chlorophenol degradation, J. Mol. Liq. 262 (2018) 194–203.
[68] Y.-R. Jiang, et al., Hydrothermal synthesis of bismuth oxybromide–bismuth oxyiodide composites with high visible light photocatalytic performance for the degradation of CV and phenol, RSC Adv. 5 (39) (2015) 30851–30860.
[69] W. Li, et al., Synthesis of rattle-type magnetic mesoporous Fe 3 O 4@ mSiO 2@ BiOBr hierarchical photocatalyst and investigation of its photoactivity in the degradation of methylene blue, RSC Adv. 5 (59) (2015) 48050–48059.
[70] Z. Liu, et al., Effect of solvents on morphology and photocatalytic activity of BiOBr synthesized by solvothermal method, Mater. Res. Bull. 47 (11) (2012) 3753–3757.
[71] T. Senasu, et al., CdS/BiOBr heterojunction photocatalyst with high performance for solar-light-driven degradation of ciprofloxacin and norfloxacin antibiotics, Appl. Surf. Sci. 567 (2021), 150850.
[72] R. Zhang, et al., Solvothermal synthesis of a peony flower-like dual Z-scheme PANI/BiOBr/ZnFe2O4 photocatalyst with excellent photocatalytic redox activity for organic pollutant under visible-light, Sep. Purif. Technol. 234 (2020), 116098.
[73] J. Zhang, et al., Improvement of visible light photocatalytic activity over flower-like BiOCl/BiOBr microspheres synthesized by reactable ionic liquids, Colloids Surf. A Physicochem. Eng. Asp. 420 (2013) 89–95.
[74] L. Cheng, X. Hu, L. Hao, Ultrasonic-assisted in-situ fabrication of BiOBr modified Bi2O2CO3 microstructure with enhanced photocatalytic performance, Ultrason. Sonochem. 44 (2018) 137–145.
[75] G. Tang, et al., Constructing novel visible-light-driven ternary photocatalyst of AgBr nanoparticles decorated 2D/2D heterojunction of g-C3N4/BiOBr nanosheets with remarkably enhanced photocatalytic activity for water-treatment, Ceram. Int. 45 (15) (2019) 19197–19205.
[76] M. Gao, et al., Surface decoration of BiOBr with BiPO4 nanoparticles to build heterostructure photocatalysts with enhanced visible-light photocatalytic activity, Sep. Purif. Technol. 170 (2016) 183–189.
[77] M. Yaghoubi-berijani, B. Bahramian, Preparation and measurement of properties of BiOBr/BiOCl/PANI ternary nanocomposite for highly efficient visible light photocatalytic applications, Res. Chem. Intermed. 47 (6) (2021) 2311–2330.
[78] Y. Zhao, et al., Fabrication of BiOBr nanosheets@ TiO2 nanobelts p–n junction photocatalysts for enhanced visible-light activity, Appl. Surf. Sci. 365 (2016) 209–217.
[79] Q. Hu, et al., Ionic liquid-induced double regulation of carbon quantum dots modified bismuth oxychloride/bismuth oxybromide nanosheets with enhanced visible-light photocatalytic activity, J. Colloid Interface Sci. 519 (2018) 263–272.
[80] S.-T. Huang, et al., Synthesis, characterization, photocatalytic activity of visible-light-responsive photocatalysts BiOxCly/BiOmBrn by controlled hydrothermal method, J. Mol. Catal. Chem. 391 (2014) 105–120.
[81] Y. Cui, et al., Photocatalytic activities of Bi2S3/BiOBr nanocomposites synthesized by a facile hydrothermal process, Appl. Surf. Sci. 290 (2014) 233–239.
[82] D.M. Blake, Bibliography of Work on the Heterogeneous Photocatalytic Removal of Hazardous Compounds from Water, National Renewable Energy Lab. (NREL), Golden, CO (United States), 1999.
[83] P. Schmitt-Kopplin, et al., Structural changes in a dissolved soil humic acid during photochemical degradation processes under O2 and N2 atmosphere, Environ. Sci. Technol. 32 (17) (1998) 2531–2541.
[84] J. Cai, et al., Bismuth oxybromide/bismuth oxyiodide nanojunctions decorated on flexible carbon fiber cloth as easily recyclable photocatalyst for removing various pollutants from wastewater, J. Colloid Interface Sci. 608 (2022) 2660–2671.
[85] Z. Jiang, et al., The hydrothermal synthesis of BiOBr flakes for visible-light-responsive photocatalytic degradation of methyl orange, J. Photochem. Photobiol. Chem. 212 (1) (2010) 8–13.
[86] H. Liu, et al., Engineering design of hierarchical g-C3N4@ Bi/BiOBr ternary heterojunction with Z-scheme system for efficient visible-light photocatalytic performance, J. Alloys Compd. 798 (2019) 741–749.
[87] W.S. Koe, et al., An overview of photocatalytic degradation: photocatalysts, mechanisms, and development of photocatalytic membrane, Environ. Sci. Pollut. Control Ser. 27 (2020) 2522–2565.
[88] A. Rafiq, et al., Photocatalytic degradation of dyes using semiconductor photocatalysts to clean industrial water pollution, J. Ind. Eng. Chem. 97 (2021) 111–128.
[89] K. Qin, et al., A review of bismuth-based photocatalysts for antibiotic degradation: insight into the photocatalytic degradation performance, pathways and relevant mechanisms, Environ. Res. 199 (2021), 111360.
[90] G. Ren, et al., Recent advances of photocatalytic application in water treatment: a review, Nanomaterials 11 (7) (2021) 1804.
[91] J.-H. Shon, T.S. Teets, Photocatalysis with transition metal based photosensitizers, Comments Mod. Chem. 40 (2) (2020) 53–85.
[92] X. Zhang, et al., Visible-light-induced photocatalytic hydrogen production over binuclear RuII–bipyridyl dye-sensitized TiO2 without noble metal loading, Chem.–Eur. J. 18 (38) (2012) 12103–12111.
[93] F. Gao, et al., Enhance the optical absorptivity of nanocrystalline TiO2 film with high molar extinction coefficient ruthenium sensitizers for high performance dye-sensitized solar cells, J. Am. Chem. Soc. 130 (32) (2008) 10720–10728.
[94] R.A. Jensen, et al., Dye-sensitized solar cells: sensitizer-dependent injection into ZnO nanotube electrodes, Langmuir 26 (3) (2010) 1401–1404.
[95] J. Zhu, et al., Graphene oxide covalently functionalized with zinc phthalocyanine for broadband optical limiting, Carbon 49 (6) (2011) 1900–1905.
[96] M. Zhang, et al., Hierarchical nanostructures of copper (II) phthalocyanine on electrospun TiO2 nanofibers: controllable solvothermal-fabrication and enhanced visible photocatalytic properties, ACS Appl. Mater. Interfaces 3 (2) (2011) 369–377.
[97] M. Yaghoubi-berijani, B. Bahramian, Synthesis, and new design into enhanced photocatalytic activity of porphyrin immobilization on the surface of bismuth oxyhalides modified with polyaniline, J. Inorg. Organomet. Polym. Mater. 30 (11) (2020) 4637–4654.
[98] S. Bai, et al., Facet-engineered surface and interface design of photocatalytic materials, Adv. Sci. 4 (1) (2017), 1600216.
[99] R.A. Rather, et al., Influence of exposed facets, morphology and hetero-interfaces of BiVO4 on photocatalytic water oxidation: a review, Int. J. Hydrogen Energy 46 (42) (2021) 21866–21888.
[100] X.-M. Cheng, J. Zhao, W.-Y. Sun, Facet-engineering of materials for photocatalytic application: status and future prospects, Energy (2022), 100084.
[101] Y.-K. Peng, S.E. Tsang, Facet-dependent photocatalysis of nanosize semiconductive metal oxides and progress of their characterization, Nano Today 18 (2018) 15–34.

[102] K. Zhou, Y. Li, Catalysis based on nanocrystals with well-defined facets, Angew. Chem. Int. Ed. 51 (3) (2012) 602–613.
[103] G. Liu, et al., Crystal facet engineering of semiconductor photocatalysts: motivations, advances and unique properties, Chem. Commun. 47 (24) (2011) 6763–6783.
[104] J. Jiang, et al., Synthesis and facet-dependent photoreactivity of BiOCl single-crystalline nanosheets, J. Am. Chem. Soc. 134 (10) (2012) 4473–4476.
[105] N. Wu, et al., Shape-enhanced photocatalytic activity of single-crystalline anatase TiO2 (101) nanobelts, J. Am. Chem. Soc. 132 (19) (2010) 6679–6685.
[106] R. Li, et al., Spatial separation of photogenerated electrons and holes among {010} and {110} crystal facets of BiVO4, Nat. Commun. 4 (1) (2013) 1–7.
[107] H. Zhang, et al., Enhanced photocatalytic properties in BiOBr nanosheets with dominantly exposed (102) facets, J. Phys. Chem. C 118 (26) (2014) 14662–14669.
[108] D. Zhang, et al., High {001} facets dominated BiOBr lamellas: facile hydrolysis preparation and selective visible-light photocatalytic activity, J. Mater. Chem. 1 (30) (2013) 8622–8629.
[109] J. Di, et al., Ultrathin two-dimensional materials for photo-and electrocatalytic hydrogen evolution, Mater. Today 21 (7) (2018) 749–770.
[110] J. Li, et al., Solar water splitting and nitrogen fixation with layered bismuth oxyhalides, Acc. Chem. Res. 50 (1) (2017) 112–121.
[111] J. Di, et al., Defect-tailoring mediated electron–hole separation in single-unit-cell Bi3O4Br nanosheets for boosting photocatalytic hydrogen evolution and nitrogen fixation, Adv. Mater. 31 (28) (2019), 1807576.
[112] S. Polarz, et al., On the role of oxygen defects in the catalytic performance of zinc oxide, Angew. Chem. Int. Ed. 45 (18) (2006) 2965–2969.
[113] K. Zhao, et al., Surface structure-dependent molecular oxygen activation of BiOCl single-crystalline nanosheets, J. Am. Chem. Soc. 135 (42) (2013) 15750–15753.
[114] Q. Wang, et al., Ultrathin two-dimensional BiOBrxI1-x solid solution with rich oxygen vacancies for enhanced visible-light-driven photoactivity in environmental remediation, Appl. Catal. B Environ. 236 (2018) 222–232.
[115] Q. Wang, et al., Oxygen vacancy-rich ultrathin sulfur-doped bismuth oxybromide nanosheet as a highly efficient visible-light responsive photocatalyst for environmental remediation, Chem. Eng. J. 360 (2019) 838–847.
[116] X. Xue, et al., Oxygen vacancy engineering promoted photocatalytic ammonia synthesis on ultrathin two-dimensional bismuth oxybromide nanosheets, Nano Lett. 18 (11) (2018) 7372–7377.
[117] J. Di, et al., Bismuth vacancy-tuned bismuth oxybromide ultrathin nanosheets toward photocatalytic CO2 reduction, ACS Appl. Mater. Interfaces 11 (34) (2019) 30786–30792.
[118] X. Tu, et al., The influence of Sn (II) doping on the photoinduced charge and photocatalytic properties of BiOBr microspheres, J. Mater. Sci. 50 (12) (2015) 4312–4323.
[119] X.C. Song, et al., The solvothermal synthesis and enhanced photocatalytic activity of Zn 2+ doped BiOBr hierarchical nanostructures, New J. Chem. 40 (1) (2016) 130–135.
[120] J. Di, et al., Bismuth oxyhalide layered materials for energy and environmental applications, Nano Energy 41 (2017) 172–192.
[121] X. Meng, et al., Enhanced visible light-induced photocatalytic activity of surface-modified BiOBr with Pd nanoparticles, Appl. Surf. Sci. 433 (2018) 76–87.
[122] J. Di, et al., Reactable ionic liquid assisted synthesis of Pd modified BiOBr flower-like microsphere with high dispersion and their enhanced photocatalytic performances, Mater. Technol. 30 (2) (2015) 113–121.
[123] Y. Wang, et al., Synergy between plasmonic and sites on gold nanoparticle-modified bismuth-rich bismuth oxybromide nanotubes for the efficient photocatalytic CC coupling synthesis of ethane, J. Colloid Interface Sci. 616 (2022) 649–658.
[124] X. Li, et al., Citric acid-assisted synthesis of nano-Ag/BiOBr with enhanced photocatalytic activity, Sci. China Chem. 58 (3) (2015) 457–466.
[125] C. Yu, et al., Novel noble metal (Rh, Pd, Pt)/BiOX (Cl, Br, I) composite photocatalysts with enhanced photocatalytic performance in dye degradation, Sep. Purif. Technol. 120 (2013) 110–122.
[126] J. Xia, et al., Synthesis of erbium ions doped BiOBr via a reactive ionic liquid with improved photocatalytic activity, Colloids Surf. A Physicochem. Eng. Asp. 489 (2016) 343–350.
[127] H. Lin, et al., Novel I−-doped BiOBr composites: modulated valence bands and largely enhanced visible light phtotocatalytic activities, Catal. Commun. 49 (2014) 87–91.
[128] Z. Liu, et al., Fe-ions modified BiOBr mesoporous microspheres with excellent photocatalytic property, Catal. Lett. 142 (12) (2012) 1489–1497.
[129] Z. Wei, et al., Novel visible-light irradiation niobium-doped BiOBr microspheres with enhanced photocatalytic performance, J. Mater. Sci. 55 (35) (2020) 16522–16532.
[130] Z. Wei, et al., Preparation of Mn-doped BiOBr microspheres for efficient visible-light-induced photocatalysis, Mrs Commun. 3 (3) (2013) 145–149.
[131] X. Lv, et al., Solvothermal synthesis of copper-doped BiOBr microflowers with enhanced adsorption and visible-light driven photocatalytic degradation of norfloxacin, Chem. Eng. J. 401 (2020), 126012.
[132] R. Wang, et al., Efficient visible-light-induced photocatalytic activity over the novel Ti-doped BiOBr microspheres, Powder Technol. 228 (2012) 258–263.
[133] K.-L. Zhang, et al., Study of the electronic structure and photocatalytic activity of the BiOCl photocatalyst, Appl. Catal. B Environ. 68 (3–4) (2006) 125–129.
[134] X. Chang, et al., BiOX (X= Cl, Br, I) photocatalysts prepared using NaBiO3 as the Bi source: characterization and catalytic performance, Catal. Commun. 11 (5) (2010) 460–464.
[135] Y. Xing, et al., New insights into photocatalytic mechanism and photoelectrochemical property of bismuth oxybromide heterostructure with DFT investigation, Appl. Surf. Sci. 458 (2018) 464–477.
[136] X. Xiao, et al., Oxygen-rich bismuth oxyhalides: generalized one-pot synthesis, band structures and visible-light photocatalytic properties, J. Mater. Chem. 22 (43) (2012) 22840–22843.
[137] C. Zheng, et al., Selective photocatalytic oxidation of benzyl alcohol into benzaldehyde with high selectivity and conversion ratio over Bi4O5Br2 nanoflakes under blue LED irradiation, Appl. Catal. B Environ. 205 (2017) 201–210.
[138] J. Di, et al., Controllable synthesis of Bi 4 O 5 Br 2 ultrathin nanosheets for photocatalytic removal of ciprofloxacin and mechanism insight, J. Mater. Chem. 3 (29) (2015) 15108–15118.
[139] X. Mao, F. Xie, M. Li, Facile hydrolysis synthesis of novel Bi4O5Br2 photocatalyst with enhanced visible light photocatalytic activity for the degradation of resorcinol, Mater. Lett. 166 (2016) 296–299.
[140] L. Ye, et al., Thickness-ultrathin and bismuth-rich strategies for BiOBr to enhance photoreduction of CO2 into solar fuels, Appl. Catal. B Environ. 187 (2016) 281–290.
[141] S. Wang, et al., Light-switchable oxygen vacancies in ultrafine Bi5O7Br nanotubes for boosting solar-driven nitrogen fixation in pure water, Adv. Mater. 29 (31) (2017), 1701774.
[142] Y. Su, et al., First hydrothermal synthesis of Bi5O7Br and its photocatalytic properties for molecular oxygen activation and RhB degradation, Appl. Surf. Sci. 346 (2015) 311–316.
[143] J. Wang, Y. Yu, L. Zhang, Highly efficient photocatalytic removal of sodium pentachlorophenate with Bi3O4Br under visible light, Appl. Catal. B Environ. 136 (2013) 112–121.
[144] K.-L. Li, et al., Synthesis of BiOBr, Bi3O4Br, and Bi12O17Br2 by controlled hydrothermal method and their photocatalytic properties, J. Taiwan Inst. Chem. Eng. 45 (5) (2014) 2688–2697.
[145] J. Shang, et al., Bismuth oxybromide with reasonable photocatalytic reduction activity under visible light, ACS Catal. 4 (3) (2014) 954–961.
[146] Y. Wang, et al., A novel ion-exchange strategy for the fabrication of high strong BiOI/BiOBr heterostructure film coated metal wire mesh with tunable visible-light-driven photocatalytic reactivity, J. Hazard Mater. 351 (2018) 11–19.
[147] X. Jia, et al., Transforming type-I to type-II heterostructure photocatalyst via energy band engineering: a case study of I-BiOCl/I-BiOBr, Appl. Catal. B Environ. 204 (2017) 505–514.
[148] J. Hu, et al., Synthesis of a hierarchical BiOBr nanodots/Bi 2 WO 6 p–n heterostructure with enhanced photoinduced electric and photocatalytic degradation performance, RSC Adv. 6 (35) (2016) 29554–29562.

[149] J. Rashid, et al., Butterfly cluster like lamellar BiOBr/TiO2 nanocomposite for enhanced sunlight photocatalytic mineralization of aqueous ciprofloxacin, Sci. Total Environ. 665 (2019) 668–677.
[150] A. Han, et al., Efficient photodegradation of chlorophenols by BiOBr/NaBiO3 heterojunctioned composites under visible light, J. Hazard Mater. 341 (2018) 83–92.
[151] X. Xie, et al., Photoinduced synthesis of green photocatalyst Fe3O4/BiOBr/CQDs derived from corncob biomass for carbamazepine degradation: the role of selectively more CQDs decoration and Z-scheme structure, Chem. Eng. J. 420 (2021), 129705.
[152] X.-X. Wei, et al., Hybrid BiOBr–TiO2 nanocomposites with high visible light photocatalytic activity for water treatment, J. Hazard Mater. 263 (2013) 650–658.
[153] X.-X. Wei, et al., Advanced visible-light-driven photocatalyst BiOBr–TiO 2–graphene composite with graphene as a nano-filler, J. Mater. Chem. 2 (13) (2014) 4667–4675.
[154] X.-j. Wang, et al., Construction of amorphous TiO2/BiOBr heterojunctions via facets coupling for enhanced photocatalytic activity, J. Hazard Mater. 292 (2015) 126–136.
[155] B. Liu, et al., Synthesis of g-C3N4/BiOI/BiOBr heterostructures for efficient visible-light-induced photocatalytic and antibacterial activity, J. Mater. Sci. Mater. Electron. 29 (16) (2018) 14300–14310.
[156] D. Yuan, et al., Synthesis and photocatalytic activity of gC 3 N 4/BiOI/BiOBr ternary composites, RSC Adv. 6 (47) (2016) 41204–41213.
[157] J. Cao, et al., Chemical etching preparation of BiOI/BiOBr heterostructures with enhanced photocatalytic properties for organic dye removal, Chem. Eng. J. 185 (2012) 91–99.
[158] D. Lv, et al., Magnetic NiFe2O4/BiOBr composites: one-pot combustion synthesis and enhanced visible-light photocatalytic properties, Sep. Purif. Technol. 158 (2016) 302–307.
[159] X. Yu, et al., A three-dimensional BiOBr/RGO heterostructural aerogel with enhanced and selective photocatalytic properties under visible light, Appl. Surf. Sci. 396 (2017) 1775–1782.
[160] X. Tu, et al., One-pot synthesis, characterization, and enhanced photocatalytic activity of a BiOBr–graphene composite, Chem.–Eur. J. 18 (45) (2012) 14359–14366.
[161] Q.W. Cao, et al., A novel CdWO4/BiOBr p–n heterojunction as visible light photocatalyst, J. Alloys Compd. 670 (2016) 12–17.
[162] X. Zou, et al., The highly enhanced visible light photocatalytic degradation of gaseous o-dichlorobenzene through fabricating like-flowers BiPO4/BiOBr pn heterojunction composites, Appl. Surf. Sci. 391 (2017) 525–534.
[163] W. An, et al., Surface decoration of BiPO4 with BiOBr nanoflakes to build heterostructure photocatalysts with enhanced photocatalytic activity, Appl. Surf. Sci. 351 (2015) 1131–1139.
[164] L. Kong, et al., Unusual reactivity of visible-light-responsive AgBr–BiOBr heterojunction photocatalysts, J. Catal. 293 (2012) 116–125.
[165] X. Su, D. Wu, Facile construction of the phase junction of BiOBr and Bi4O5Br2 nanoplates for ciprofloxacin photodegradation, Mater. Sci. Semicond. Process. 80 (2018) 123–130.
[166] P. Li, et al., NaOH-induced formation of 3D flower-sphere BiOBr/Bi4O5Br2 with proper-oxygen vacancies via in-situ self-template phase transformation method for antibiotic photodegradation, Sci. Total Environ. 715 (2020), 136809.
[167] Y. Guo, et al., In situ crystallization for fabrication of a core–satellite structured BiOBr–CdS heterostructure with excellent visible-light-responsive photoreactivity, Nanoscale 7 (27) (2015) 11702–11711.
[168] Z.S. Liu, et al., BiPO4/BiOBr p–n junction photocatalysts: one-pot synthesis and dramatic visible light photocatalytic activity, Mater. Res. Bull. 63 (2015) 187–193.
[169] J. Wang, et al., Novel three-dimensional flowerlike BiOBr/Bi2SiO5 p–n heterostructured nanocomposite for degradation of tetracycline: enhanced visible light photocatalytic activity and mechanism, ACS Sustain. Chem. Eng. 6 (11) (2018) 14221–14229.
[170] L. Wang, et al., Facile construction of novel BiOBr/Bi12O17Cl2 heterojunction composites with enhanced photocatalytic performance, J. Colloid Interface Sci. 560 (2020) 21–33.
[171] H. Liu, et al., One-pot hydrothermal synthesis of SnO2/BiOBr heterojunction photocatalysts for the efficient degradation of organic pollutants under visible light, ACS Appl. Mater. Interfaces 10 (34) (2018) 28686–28694.
[172] C. Liu, et al., Layered BiOBr/Ti3C2 MXene composite with improved visible-light photocatalytic activity, J. Mater. Sci. 54 (3) (2019) 2458–2471.
[173] S. Wang, et al., A plate-on-plate sandwiched Z-scheme heterojunction photocatalyst: BiOBr-Bi2MoO6 with enhanced photocatalytic performance, Appl. Surf. Sci. 391 (2017) 194–201.
[174] D. Wu, et al., Alkali-induced in situ fabrication of Bi2O4-decorated BiOBr nanosheets with excellent photocatalytic performance, J. Phys. Chem. C 120 (14) (2016) 7715–7727.
[175] S. Fu, et al., A novel 0D/2D WS2/BiOBr heterostructure with rich oxygen vacancies for enhanced broad-spectrum photocatalytic performance, J. Colloid Interface Sci. 569 (2020) 150–163.
[176] J. Di, et al., New insight of Ag quantum dots with the improved molecular oxygen activation ability for photocatalytic applications, Appl. Catal. B Environ. 188 (2016) 376–387.
[177] J. Fu, et al., BiOBr–carbon nitride heterojunctions: synthesis, enhanced activity and photocatalytic mechanism, J. Mater. Chem. 22 (39) (2012) 21159–21166.
[178] X.-J. Wen, et al., Facile synthesis of a visible light α-Fe 2 O 3/BiOBr composite with high photocatalytic performance, RSC Adv. 6 (5) (2016) 4035–4042.
[179] S. Shenawi-Khalil, et al., A novel heterojunction BiOBr/bismuth oxyhydrate photocatalyst with highly enhanced visible light photocatalytic properties, J. Phys. Chem. C 116 (20) (2012) 11004–11012.
[180] T. Hu, et al., A novel Z-scheme Bi2MoO6/BiOBr photocatalyst for enhanced photocatalytic activity under visible light irradiation, Appl. Surf. Sci. 456 (2018) 473–481.
[181] M. Ji, et al., Enhanced photocatalytic performance of carbon quantum dots/BiOBr composite and mechanism investigation, Chin. Chem. Lett. 29 (6) (2018) 805–810.
[182] S. Guan, et al., Preparation and promising application of novel LaFeO3/BiOBr heterojunction photocatalysts for photocatalytic and photo-Fenton removal of dyes, Opt. Mater. 100 (2020), 109644.
[183] X. Li, et al., Novel BP/BiOBr S-scheme nano-heterojunction for enhanced visible-light photocatalytic tetracycline removal and oxygen evolution activity, J. Hazard Mater. 387 (2020), 121690.
[184] Y. Geng, et al., Preparation, characterization and photocatalytic properties of BiOBr/ZnO composites, J. Energy Chem. 26 (3) (2017) 416–421.
[185] Q.-Y. Tang, et al., Enhanced photocatalytic degradation of glyphosate over 2D CoS/BiOBr heterojunctions under visible light irradiation, J. Hazard Mater. 407 (2021), 124798.
[186] T. Xie, et al., Visible-light-driven photocatalytic activity of magnetic BiOBr/SrFe12O19 nanosheets, Nanomaterials 9 (5) (2019) 735.
[187] X. Zou, et al., Lanthanum orthovanadate/bismuth oxybromide heterojunction for enhanced photocatalytic air purification and mechanism exploration, Chem. Eng. J. 379 (2020), 122380.
[188] J. Xia, et al., Improved visible light photocatalytic activity of MWCNT/BiOBr composite synthesized via a reactable ionic liquid, Ceram. Int. 40 (3) (2014) 4607–4616.
[189] T. Jia, et al., A facile approach for the synthesis of Zn2SnO4/BiOBr hybrid nanocomposites with improved visible-light photocatalytic performance, Nanomaterials 8 (5) (2018) 313.
[190] K.-L. Jia, et al., BiOBr/Ag6Si2O7 heterojunctions for enhancing visible light catalytic degradation performances with a sequential selectivity enabled by dual synergistic effects, J. Colloid Interface Sci. 561 (2020) 396–407.
[191] J. Zhang, et al., One-step growth of nanosheet-assembled BiOCl/BiOBr microspheres for highly efficient visible photocatalytic performance, Appl. Surf. Sci. 430 (2018) 639–646.
[192] Y. Xue, et al., Efficient degradation of atrazine by BiOBr/UiO-66 composite photocatalyst under visible light irradiation: environmental factors, mechanisms and degradation pathways, Chemosphere 203 (2018) 497–505.

[193] Y. Ao, et al., Synthesis of novel 2D-2D pn heterojunction BiOBr/La2Ti2O7 composite photocatalyst with enhanced photocatalytic performance under both UV and visible light irradiation, Appl. Catal. B Environ. 194 (2016) 157–168.
[194] Y. Ao, et al., A novel p–n heterostructured photocatalyst for the efficient photocatalytic degradation of different kinds of organic compounds under irradiation of both ultraviolet and visible light, Dalton Trans. 45 (35) (2016) 13907–13916.
[195] S.-R. Zhu, et al., Hierarchical core–shell SiO 2@ PDA@ BiOBr microspheres with enhanced visible-light-driven photocatalytic performance, Dalton Trans. 46 (34) (2017) 11451–11458.
[196] M. Pálmai, et al., Pd-decorated m-BiVO 4/BiOBr ternary composite with dual heterojunction for enhanced photocatalytic activity, J. Mater. Chem. 5 (2) (2017) 529–534.
[197] H. Li, et al., Visible-light-driven Z-scheme rGO/Bi 2 S 3–BiOBr heterojunctions with tunable exposed BiOBr (102) facets for efficient synchronous photocatalytic degradation of 2-nitrophenol and Cr (VI) reduction, Environ. Sci. J. Integr. Environ. Res.: Nano 6 (12) (2019) 3670–3683.
[198] N. Alikhani, et al., Photocatalytic degradation and adsorption of herbicide 2, 4-dichlorophenoxyacetic acid from aqueous solution using TiO2/BiOBr/Bi2S3 nanostructure stabilized on the activated carbon under visible light, Environ. Nanotechnol. Monit. Manag. 15 (2021), 100415.
[199] K. Perumal, et al., Construction of Ag2CO3/BiOBr/CdS ternary composite photocatalyst with improved visible-light photocatalytic activity on tetracycline molecule degradation, J. Environ. Sci. 125 (2023) 47–60.
[200] J. Wang, et al., A novel Bi2WO6/BiOBr/RGO photocatalyst for enhanced degradation of ciprofloxacin under visible light irradiation: performance, mechanism and toxicity evaluation, Diam. Relat. Mater. 128 (2022), 109274.
[201] J. Li, et al., Insight into the enhanced visible-light photoreduction of aqueous Cr (VI) by assembled Fe3O4/LDO/BiOBr composites, Colloids Surf. A Physicochem. Eng. Asp. 634 (2022), 128021.
[202] A. Chachvalvutikul, T. Luangwanta, S. Kaowphong, Double Z-scheme FeVO4/Bi4O5Br2/BiOBr ternary heterojunction photocatalyst for simultaneous photocatalytic removal of hexavalent chromium and rhodamine B, J. Colloid Interface Sci. 603 (2021) 738–757.